Uncontrolled CD21^{low} age-associated and B1 B cell accumulation caused by failure of an EGR2/3 tolerance checkpoint

Authors:

Etienne Masle-Farquhar [1,2], Timothy J. Peters [1,2], Lisa A. Miosge [3], Ian A. Parish [4,5], Christoph Weigel[6], Christopher C. Oakes[6], Joanne H. Reed [1,2,#], Christopher C. Goodnow [1,7,#*]

Affiliations:

[1] The Garvan Institute of Medical Research, Darlinghurst, Sydney, NSW 2010, Australia.

[2] St Vincent's Clinical School, UNSW Sydney, 2052, Australia.

[3] Department of Immunology and Infectious Disease, John Curtin School of Medical Research, Australian National University, Canberra, Australia.

[4] Cancer Immunology Program, Peter MacCallum Cancer Centre, VIC 3000, Australia

[5] Sir Peter MacCallum Department of Oncology, The University of Melbourne, Parkville, VIC 3052, Australia.

[6] Division of Hematology, Department of Internal Medicine, The Ohio State University, Columbus, Ohio, USA.

[7] Cellular Genomics Futures Institute, UNSW Sydney, Australia

[#] Equal senior authors.

[*] Correspondence: c.goodnow@garvan.org.au

SUMMARY

CD21^{low} age-associated or atypical memory B cells, enriched for autoantibodies and poised for plasma cell differentiation, accumulate in large numbers in chronic infections, autoimmune disease and immunodeficiency, posing the question of what checkpoints normally oppose their excessive accumulation. Here, we reveal a critical role for the calcium-NFAT-regulated transcription factors EGR2 and EGR3. In the absence of EGR2 and EGR3 within B cells, CD21^{low} and B1 B cells accumulate and circulate in young mice in numbers 10-20 times greater than normal, over-express a large set of EGR2 ChIP-seq target genes including known drivers of plasma cell differentiation and under-express drivers of follicular germinal centers. Most follicular B cells constitutively express *Egr2* proportionally to surface IgM down-regulation by self-antigens, and EGR2/3 deficiency abolishes this characteristic anergy response. These results define a key transcriptional checkpoint repressing CD21^{low} B cell formation and inform how *NFATC1* or *EGR2* mutations promote B1 cell-derived chronic lymphocytic leukemias.

Keywords:

CD21^{low} B cell, age-associated B cell, atypical-memory B cell, double-negative B cell, B1 B cell, EGR2, EGR3, CLL, tolerance, anergy.

INTRODUCTION

Atypical CD21^{low} B cell populations accumulate in large numbers in multiple disease states, but little is known about the physiological checkpoints normally opposing their formation. These cells, variously labelled atypical-memory, IgD/CD27 double-negative, age-associated or CD21^{low} B cells, share the unusual loss of cell-surface CR2 complement C3d receptor (CD21) expression, and display gene expression and antibody V-region profiles intermediate between

follicular or memory B cells on the one hand, and plasmablasts on the other (Charles et al., 2011, Isnardi et al., 2010, Jenks et al., 2018, Rakhmanov et al., 2009, Rubtsov et al., 2011, Russell Knode et al., 2017, Terrier et al., 2011, Scharer et al., 2019). We refer to them collectively here as CD21^{low} B cells.

Atypical CD21^{low} B cells were first found accumulating in individuals with human immunodeficiency virus (HIV) chronic viremia (Benedetto et al., 1992, Moir et al., 2001), and contain the majority of cells bearing immunoglobulin against HIV envelope gp120 (Moir et al., 2008). CD21^{low} B cells also accumulate in individuals with common variable immunodeficiency (CVID) and concomitant autoimmune cytopenias (Isnardi et al., 2010, Warnatz et al., 2002) or severe systemic lupus erythematosus (SLE) (Rakhmanov et al., 2009, Wei et al., 2007). CD21^{low} B cells that accumulate with chronic HCV infections often express rheumatoid factor IgM that binds self-IgG (Charles et al., 2011, Terrier et al., 2011) and in CVID and lupus, many CD21^{low} B cells express self-reactive *IGHV4-34* immunoglobulins (Rakhmanov et al., 2009, Wei et al., 2007). CD21^{low} CD23^{low} B cells, many expressing anti-chromatin immunoglobulins (Russell Knode et al., 2017), accumulate in the archetypal systemic autoimmune mouse strain, NZB/W, in *Mertk*$^{-/-}$ mice genetically predisposed to lupus-like autoimmunity, or in old C57BL/6 mice without overt autoimmune disease (Hao et al., 2011, Rubtsov et al., 2011).

Here, we reveal the critical role in opposing CD21^{low} B cell accumulation served by Early Growth Response 2 (EGR2) and EGR3. These paralogous zinc finger transcription factors are encoded by immediate early genes that are induced by chronic self-antigen stimulation of cell-surface IgM and IgD through calcium- and calcineurin-activated transcription factors of the nuclear factor of activated T cells (NFAT) family (Healy et al., 1997, Glynne et al., 2000, Merrell et al., 2006, Sabouri et al., 2016, Marklin et al., 2017). The function of EGR2 and EGR3 in B cells is not known, as earlier knockout mouse studies were confounded by their essential

roles in T cells (Li et al., 2012). *EGR2* is induced in CD21^{low} B cells in humans (Isnardi et al., 2010, Terrier et al., 2011) and mice (Russell Knode et al., 2017), and somatic missense *EGR2* mutations recur and predict poor outcome in B cell chronic lymphocytic leukemia (CLL)(Young et al., 2017). CLLs display constitutive NFAT activation(Schuh et al., 1996), resemble self-reactive anergic B cells, and derive from another chronically-stimulated self-reactive population – B1 cells(Apollonio et al., 2013). Like CD21^{low} B cells, B1 cells also accumulate in large numbers in NZBW autoimmunity-prone mice (Hayakawa et al., 1983). *EGR2* is also induced by *acute* BCR stimulation to promote B cell proliferation *in vitro* (Glynne et al., 2000, Li et al., 2012, Newton et al., 1996), highlighting the question of what functions EGR2 and EGR3 perform in B cells *in vivo*.

Here, we studied the functions of EGR2/3 in B cells *in vivo* by analysing chimeric mice with *Egr2* and *Egr3* deletion restricted to a fraction of B cells. This revealed a critical, cell-autonomous function for EGR2/EGR3 in repressing formation of CD21^{low} and B1 B cell populations, and in promoting the IgM^{low} IgD^{high} anergy response of self-reactive follicular B cells. Using flow cytometry and single-cell RNA sequencing, we define the landscape of EGR2/EGR3-repressed and -induced genes in CD21^{low}, B1a and follicular B cells, many corresponding to EGR2 chromatin immunoprecipitation sequencing (ChIP-seq) targets in CLL. Our findings define a critical EGR2/EGR3 transcriptional checkpoint governing accumulation of CD21^{low} and B1 B cells and reveal the molecular circuit responsible for the cardinal features of anergic B cells.

RESULTS

Egr2 and Egr3 repress mature CD21^{low} CD23^{low} B cells.

To study the functions of *Egr2* and *Egr3* in B cells, we intercrossed germline *Egr3* knockout mice with mice expressing a loxP-flanked *Egr2* allele and a *Cre* transgene controlled by the

Cd19 promoter, resulting in B cell-specific *Egr2* deletion. All mice examined were matched for *Cd19*$^{Cre/+}$ and we thus describe *Egr2*^{fl} *Egr3*^{KO} mice based only on their *Egr2* and *Egr3* genotypes.

Mice lacking one or both alleles of *Egr2* and/or *Egr3* in B cells had no changes in the bone marrow with respect to mean frequency or number of precursor B cells, immature B cells or mature recirculating B cells (**Supplementary Figure 1A,B**). In the spleen, *Egr2*$^{fl/fl}$ *Egr3*$^{KO/KO}$ mice had a 3-fold increase in mean number of CD93^{pos} CD23^{neg} immature T1 B cells (**Supplementary Figure 1C**), many of them with low cell-surface IgM expression (**Supplementary Figure 1D**).

The most striking abnormality in the spleen of *Egr2*$^{fl/fl}$ *Egr3*$^{KO/KO}$ mice was a 30- and 10-fold increase in mean frequency and number of B220^{pos} CD19^{pos} CD95^{neg} CD93^{neg} mature B cells with a CD21^{low} CD23^{low} phenotype (**Figure 1A,B**). Other B cell (CD19^{pos}) subsets that can express low levels of CD21 and CD23 were excluded from this analysis: B1a cells (B220^{int} CD5^{high} CD43^{high} CD23^{low}), germinal centre B cells (IgD^{neg} CD38^{low} CD95^{pos}) and immature B cells (CD93^{pos}). CD21^{low} CD23^{low} mature B cells were also expanded a mean 16-fold in the blood (**Figure 1C**) and 5-fold in the bone marrow (**Supplementary Figure 2A**) of *Egr2*$^{fl/fl}$ *Egr3*$^{KO/KO}$ relative to wild-type mice. A subtle increase in CD21^{low} CD23^{low} mature B cells occurred in *Egr2*$^{fl/fl}$ *Egr3*$^{KO/+}$ mice retaining one functional *Egr3* allele, but homozygous loss of *Egr2* or *Egr3* alone had no discernible effect (**Figure 1B,C; Supplementary Figure 2A**). The mean numbers of mature follicular and marginal zone B cells were normal in *Egr2*$^{fl/fl}$ *Egr3*$^{KO/KO}$ mice (**Figure 1B**), but mean cell-surface CD23 and CD21 expression were decreased on mature recirculating B cells in the bone marrow, and on immature T2 and T3 cells and splenic follicular B cells in the spleen of *Egr2*$^{fl/fl}$ *Egr3*$^{KO/KO}$ mice (**Supplementary Figure 2B**).

The accumulation of CD21^{low} CD23^{low} cells in *Egr2*$^{fl/fl}$ *Egr3*$^{KO/KO}$ mice could reflect indirect effects of *Egr3* deficiency in non-hematopoietic cells. To address this, we generated “100%

chimeras" by irradiating *Rag1*$^{KO/KO}$ mice and transplanting bone marrow from an *Egr2*$^{fl/fl}$ *Egr3*$^{KO/KO}$ mouse or from *Egr2*$^{+/+}$ *Egr3*$^{+/+}$ or *Egr2*$^{fl/+}$ *Egr3*$^{KO/+}$ control donors. *Egr2*$^{fl/fl}$ *Egr3*$^{KO/KO}$ marrow recipients had no significant change in frequency of immature or mature B cells (**Supplementary Figure 3A**), but had an 8-fold and 10-fold increase in mean frequency of CD21^{low} CD23^{low} B cells in the spleen and bone marrow, respectively (**Supplementary Figure 3B**). Homozygous *Egr2* and *Egr3* deficiency restricted to B cells and hematopoietic cells is therefore sufficient to cause accumulation of CD21^{low} CD23^{low} B cells.

To determine the *B cell*-intrinsic effects of *Egr2* and *Egr3* deficiency, we generated mixed chimeras by irradiating *Rag1*$^{KO/KO}$ mice and transplanting an equal mixture of "test" bone marrow from *Ptprc*$^{b/b}$ *Cd19*$^{Cre/+}$ mice lacking one or both alleles of *Egr2* and *Egr3* and control bone marrow from *Ptprc*$^{a/a}$ *Cd19*$^{+/+}$ *Egr2*$^{+/+}$ *Egr3*$^{+/+}$ donors (lower panel in **Figure 1D**). As an additional control, some mixed chimeras received *Ptprc*$^{b/b}$ *Cd19*$^{Cre/+}$ "test" marrow with wild-type *Egr2* and *Egr3* genes (upper panel in **Figure 1D**). We stained cells in the reconstituted chimeras with antibodies to CD45.1 or CD45.2 (encoded by *Ptprc*^{a} or *Ptprc*^{b}, respectively) and applied an identical gating strategy for CD45.1^{pos} control leukocytes and CD45.2^{pos} test leukocytes. CD45.2+ B cells with homozygous *Egr2* and *Egr3* deletion accumulated in the spleen in greater numbers than CD45.1+ wild-type control B cells in the same animal (**Figure 1E**). In addition, we observed a 20-fold accumulation of CD21^{low} CD23^{low} B cells restricted to cells lacking EGR2 and EGR3 (**Figure 1F, G**), establishing that these transcription factors act cell-autonomously to inhibit this atypical B cell population.

To determine the relative effects of *Egr2* versus *Egr3* deletion on CD21^{low} CD23^{low} B cell accumulation, we combined data from a series of mixed chimera experiments. Heterozygous *Egr2* or *Egr3* deletion alone or combined, and homozygous *Egr2* deficiency coupled with heterozygous *Egr3* deletion, were insufficient to expand CD21^{low} CD23^{low} B cells when compared to the additional control of *Ptprc*$^{b/b}$ *Cd19*$^{Cre/+}$ *Egr2*$^{+/+}$ *Egr3*$^{+/+}$ marrow recipients

(**Figure 1H**). However, homozygous *Egr3* deletion combined with heterozygous, and to a greater extent homozygous, *Egr2* deletion was sufficient for a dramatic, cell-autonomous increase in CD21^{low} CD23^{low} B cells (**Figure 1H**). Together, these data demonstrate that *Egr2* and *Egr3* act redundantly, in a cell-intrinsic manner, to suppress the accumulation of CD21^{low} CD23^{low} B cells.

EGR2/3-deficient CD21^{low} CD23^{low} cells share gene expression profiles with CD21^{low} age- and disease-associated B cells.

We performed single-cell RNA sequencing analysis on follicular, CD21^{low} CD23^{low}, and B1a CD45.1^{+} or CD45.2^{+} B cells sorted by fluorescence-activated cell sorting (FACS) from the mixed chimeras above (**Figure 2A, Supplementary Figure 4A**). Cell type and *Egr2/Egr3* genotype were the main components of gene expression variation between sorted populations (**Figure 2B, Supplementary Figure 4B**). We began by comparing CD21^{low} CD23^{low} B cells to mature follicular B cells, irrespective of *Egr2*/*Egr3* genotypes. The sorted CD21^{low} CD23^{low} B cells differentially expressed many genes previously associated with CD21^{low} atypical B cells in humans and mice (Benedetto et al., 1992, Moir et al., 2001, Moir et al., 2008, Isnardi et al., 2010, Moratto et al., 2006, Warnatz et al., 2002, Hao et al., 2011, Rubtsov et al., 2011, Charles et al., 2011, Terrier et al., 2011, Rakhmanov et al., 2009, Wei et al., 2007, Jenks et al., 2018, Lau et al., 2017, Russell Knode et al., 2017, Rubtsova et al., 2015): increased expression of *Zbtb32*, *Fcrl5*, *Sox5, Gas7, Itgam, Cd19, Cd86, Cd80, Zeb2, Lgals1, Fcgr2b, Irf4, Prdm1, Pdcd1* and decreased expression of *Cr2* (CD21), *Fcer2a* (CD23), *Sell* (CD62L), *Icosl, Ighd, Patj, Il4ra, Cd69, Irf8, Bach2, Ets1, Traf5* (**Figure 2C, D**). The CD21^{low} CD23^{low} B cells appeared poised for antibody secretion based on elevated expression of genes that promote plasma cell differentiation (*Zbtb32, Irf4, Zbtb20* and *Prdm1*) and decreased expression of genes that repress plasma cell differentiation (*Bach2, Ets1*). Gene set

enrichment analysis (GSEA) comparing the sorted CD21^{low} CD23^{low} and follicular B cells revealed a high skew (family-wise error rate, FWER, p = 0.000-0.013) towards most genes in sets previously defined as differentially expressed in age-associated B cells (B220^{+} CD93^{-} CD43^{-} CD21^{-} CD23^{-} in GSE81650 (Russell Knode et al., 2017); B220^{+} CD19^{+} CD11b^{+} in GSE28887 (Rubtsov et al., 2011)) compared to follicular B cells (**Figure 2E, Supplementary Figure 4C, Supplementary Tables 1&2**). At the leading edge of genes increased in CD21^{low} CD23^{low} B cells were genes increased in both studies of age-associated B cells: *Bhlhe41, Capn2, Sox5, Adora2a, Fah, Rhobtb1, Sirpa, Timp2, Aldh3b1, Adssl1, Gas7, Rbm47, Pon3, Sspn, Zbtb32, Spaca9, Racgap1, Itgb1, Ak8, Cd9, Itgam, Lgals1, Cd300lf, Adgre1, Cdk14*. At the leading edge of genes decreased in CD21^{low} CD23^{low} B cells were genes decreased in both studies of age-associated B cells *Fcer2a, Bmyc, Gpr174, Tnik, Rapgef4, Tmem108, Cr2, Fchsd2, Zfp318, Satb1, Trim59, Crisp3, Pxk, Lrrk2, Dusp4, Sesn1, Neurl3, Mapk11, Sell, Bnip3, Car2, Rasgef1b, Zfp608, Samsn1, Lfng, Pip5k1b.* These data demonstrate that the CD21^{low} CD23^{low} cells sorted from our mixed chimeras resemble CD21^{low}/age-associated/atypical memory B cells reported previously in mice and humans. We therefore refer to them hereafter as CD21^{low} B cells.

We next tested for differential mRNA expression between *Egr2$^{fl/fl}$ Egr3$^{KO/KO}$* (dKO) and wild-type (WT) sorted CD21^{low} B cells exposed to an identical microenvironment. This revealed the cell-intrinsic effects of *Egr2*/*Egr3* deficiency in CD21^{low} B cells. The transcriptome of dKO cells differed significantly from that of WT cells, such that cell type and *Egr2/Egr3* genotype described the two principal components of variation in pseudo-bulk analysis between samples (**Supplementary Figure 4B**). Differentially expressed genes with FWER < 0.05 comprised of 798 increased and 2687 decreased genes, in dKO relative to WT CD21^{low} B cells (**Figure 3A; Supplementary Tables 3&4**).

Somatic *EGR2* mutations (Damm et al., 2014, Young et al., 2017) and low CD21 expression (Nichols et al., 2015) both correlate with poor prognosis in CLL. To infer which differentially

196 expressed genes in dKO CD21^{low} B cells are direct EGR2 transcriptional targets in B cells, we
197 queried these genes for proximity to EGR2 ChIP-Seq binding domains, with proximity defined
198 as within 2kb from each gene's transcription start site (TSS), in at least one of two
199 independent human *EGR2*-unmutated CLL samples. On this basis, 362 of the 798 upregulated
200 genes (odds ratio; OR=1.60) and 1602 of the 2687 downregulated genes (OR=1.60) in dKO
201 CD21^{low} B cells have evidence of EGR2 binding in human B cells (**Figure 3B, Supplementary**
202 **Table 5**). The EGR2 target genes most up-regulated by EGR2/3 deficiency – and hence
203 normally repressed by EGR2/3 - were *Zbtb32, Emb, Atxn1, Lysmd2, Cpd, Cish, Tbc1d9, Il6st,*
204 *Specc1, Zbtb20* (**Figure 3C**). The EGR2 target genes most down-regulated by EGR2/3
205 deficiency – and hence normally induced by EGR2/3 - were *Wnt10a, Vpreb3, Il4i1, Lef1, Nrxn2,*
206 *Map2, Nrgn, Gm16867, Tsc22d1, Fcer2a, Id3*. Many of these direct targets correspond to genes
207 previously identified as differentially expressed by CD21^{low} B cells in mice and humans (Jenks
208 et al., 2018, Rakhmanov et al., 2009, Rubtsov et al., 2011, Russell Knode et al., 2017, Warnatz
209 et al., 2002). Our findings establish EGR2 and EGR3 as major repressors and inducers of gene
210 expression in CD21^{low} B cells.

211

212 **EGR2 and EGR3 drive the IgM^{low} IgD^{high} phenotype of self-reactive follicular B cells.**

213 Since CD21^{low} B cells in human lupus derive in part from activated follicular B cells (Scharer et
214 al., 2019), we next analysed the expression and role of EGR2 in follicular B cells. Flow
215 cytometric analysis of spleen cells from *Egr2$^{IRES\text{-}GFP}$* targeted knock-in reporter mice compared
216 to negative control *Egr2^{WT}* mice revealed that the *Egr2* gene is expressed in a large fraction of
217 follicular B cells, correlating inversely with the expression of IgM on their plasma membrane
218 (**Figure 4A**). Cells with highest *Egr2*-GFP expression had the lowest surface IgM whereas
219 there was little detectable *Egr2*-GFP expression in cells with highest surface IgM. The same
220 inverse correlation between *Egr2*-GFP expression and surface IgM existed in immature T1

and transitional T2/3 B cells (**Supplementary Fig 5A**). *Egr2*-GFP expression was higher in B cells from the lowest quartile for cell-surface IgM relative to those from the highest quartile (**Figure 4A, Supplementary Figure 5B, C**). Low cell-surface IgM and high cell surface IgD are due to self-reactivity of the expressed immunoglobulin on mouse and human B cells (Duty et al., 2009, Goodnow et al., 1989, Quach et al., 2011). This finding, that surface IgM down-regulation is a proxy for *Egr2* expression in follicular B cells, extends to single cells in the normal mouse B cell repertoire a previous finding from transgenic mice – that surface IgM is down-regulated and *Egr2* induced as a consequence of chronic binding to self-antigens (Glynne et al., 2000).

To test for a mechanistic link between *Egr2* expression and low surface IgM, we compared cell-surface IgM and IgD on $Egr2^{fl/fl}$ $Egr3^{KO/KO}$ dKO and WT follicular B cells co-existing within mixed chimeric mice. Down-regulation of IgM on most follicular B cells was abolished cell-intrinsically on dKO follicular B cells (**Figure 4B,C; Supplementary Figure 6**), accompanied by a more subtle decrease in IgD.

To explore how loss of EGR2/3 causes increased surface IgM, we compared single-cell RNA sequencing data from dKO and WT follicular B cells from mixed chimeras. This revealed 128 increased and 268 decreased genes in dKO follicular B cells with FWER $p<0.05$ (**Figure 4D, Supplementary Tables 6&7**). Of the 128 increased genes, 34 had EGR2 CHIPseq peaks within 2kb of their TSS in human CLL B cells (**Figure 4E, Supplementary Table 8**, OR=0.81). Of these 34 genes, the 24 genes with the greatest increase in dKO follicular cells (**Figure 4F)** were also all increased in dKO $CD21^{low}$ B cells. Of the 268 genes decreased in dKO follicular B cells, 146 had EGR2 CHIPseq peaks within 2kb of their TSS (**Supplementary Table 8**, OR=1.31). 20 of the 24 most decreased EGR2 target genes in dKO follicular B cells (**Figure 4F)** were also decreased in dKO $CD21^{low}$ B cells, including *Zfp318* (**Supplementary Figure 6B**). ZFP318 promotes alternative mRNA splicing of the immunoglobulin heavy chain variable

(VDJ_H) exon to *Ighd* constant region exons instead of the *Ighm* exons, and null or partial loss-of-function *Zfp318* mutations result in aberrantly high surface IgM expression due to increased *Ighm* mRNA and loss of competing IgD protein during assembly with CD79αβ (Enders et al., 2014). Consistent with diminished *Zfp318* in dKO follicular B cells, *Ighd* mRNA was also among the decreased gene set (**Supplementary Table 7**).

Collectively, the data above indicate that *Egr2* induction by chronic self-antigen binding in follicular B cells promotes transcription of *Zfp318* to decrease IgM and increase IgD, driving the IgM^{low} IgD^{high} response characteristic of anergic B cells (Duty et al., 2009, Goodnow et al., 1989, Merrell et al., 2006, Quach et al., 2011).

EGR2 and EGR3 repress B1 cells.

B1 B cells exhibit chronic signalling through self-reactive BCRs (Wong et al., 2002, Okamoto et al., 1992, Hayakawa et al., 1999, Graf et al., 2019) and comprise the majority of lymphocytes in the peritoneal cavity, but are infrequent in the circulation and spleen of most mouse strains except the autoimmune prone NZB and NZB/W strains (Hayakawa et al., 1983). Compared to wild-type controls, the mean number of peritoneal $CD5^{pos}$ B1a and $CD5^{neg}$ B1b cells was increased 15- and 16-fold, respectively, in $Egr2^{fl/fl}$ $Egr3^{KO/KO}$ mice (**Figure 5A**). A 7-fold increase in mean B1a and B1b cell numbers occurred in $Egr2^{fl/fl}$ $Egr3^{KO/+}$ but not in $Egr2^{fl/fl}$ $Egr3^{+/+}$ mice (**Figure 5A**). $Egr2^{fl/fl}$ $Egr3^{KO/KO}$ mice also had a large increase in mean number of $CD19^{pos}$ $B220^{int}$ $CD23^{low}$ $CD43^{high}$ $CD11b^{high}$ $CD5^{pos}$ B1a cells in the spleen, bone marrow and blood (**Figure 5B**). In mixed chimeras, there was a 30- and 12-fold increase in mean number of $Egr2^{fl/fl}$ $Egr3^{KO/KO}$ dKO relative to $Egr2^{+/+}$ $Egr3^{+/+}$ WT peritoneal B1a and B1b cells, respectively (**Figure 5C,D**). $Egr2^{fl/fl}$ $Egr3^{KO/KO}$ B1a cells were also increased 25-fold relative to their wild-type counterparts in the spleen and blood of mixed chimeras (**Figure 5E**).

Single cell RNA sequencing of dKO and WT B1a B cells sorted from the spleens of mixed chimeras (**Figure 2A,B**) revealed 1667 genes increased and 1783 genes decreased in dKO B1a cells (FWER < 0.05, **Supplementary Tables 9&10**). Strikingly, 354 of 924 genes increased (log2 fold change; log2FC > 0.3) and 257 of 701 genes decreased (log2FC < -0.3) in dKO B1a cells were also differentially expressed using the same threshold in dKO CD21^{low} B cells (**Figure 6A**). Both dKO populations expressed higher levels of genes up-regulated in splenic and peritoneal cavity B1a cells relative to other murine B cell subsets: *Apoe*, *Ahr*, *Adm, Cd5, Ctla4, Itgb1, Sox5, Zbtb32.* These populations also had lower expression of genes normally up-regulated upon surface immunoglobulin expression in immature B cells, or as immature B cells develop into follicular B cells, including *Il4il, Zfp318, Xkex, Il21r, Icosl, Fcshd2, Nfkb2*. Notably, EGR2/3-deficient dKO B1a and CD21^{low} B cells overexpressed a set of EGR2-ChIP-seq target genes that are normally increased in cells poised for plasma cell differentiation: *Zbtb32*, *Zbtb20*, *Mzb1*, *Il6st*, *Il6ra*, *Pim1*, *Lgals1*, and *Nfatc1*. More than half of the up-regulated (OR=1.36) or down-regulated (OR=1.60) genes in dKO B1a cells had EGR2 ChIP-seq peaks within 2 kb of their transcription start site in human CLL B cells (**Figure 6B, Supplementary Tables 11**). 253 genes had EGR2 ChIP-seq peaks within 2 kb of their TSS and were increased (log2FC > 0) in both dKO populations, and 617 genes had EGR2 ChIP-seq peaks within 2 kb of their TSS and were decreased (log2FC < 0) in both dKO populations (**Figure 6C**).

Collectively, these data demonstrate that EGR2 and EGR3 are critical regulators of B1a cells, and that the landscape of genes regulated by the EGR2/EGR3 checkpoint is similar in B1a and CD21^{low} disease-associated B cells.

DISCUSSION

Our findings reveal EGR2 and EGR3 as critical regulators of chronically-stimulated B cell populations enriched for self-reactive BCR specificities: IgM^{low} anergic follicular, CD21^{low} and

B1a B cells. We reveal that EGR2/EGR3 are essential inducers and repressors of many genes in B cells, particularly essential to repressing a suite of genes that are highly expressed in disease-associated CD21^{low} B cells and drive plasmablast differentiation. These findings and their implications for dysregulated accumulation of CD21^{low} and B1 cells in autoimmune disease and CLL are discussed below.

In mature follicular B cells, which account for the majority of "naïve" (yet to be stimulated by antigen) circulating B cells, a GFP reporter inserted into the 3' untranslated region of *Egr2* revealed that many are not naïve as they have induced the reporter. Signalling by cell-surface IgM in response to self-antigens, varying in strength from cell to cell, is the most likely stimulus because *Egr2*-GFP induction is correlated with down-regulation of surface IgM. Self-reactive follicular B cells actively down-regulate their surface IgM and activate a state of anergy proportionally to the fraction of their surface Ig molecules chronically engaged by self-antigen (Goodnow et al., 1989). Similar conclusions have been reached using a GFP reporter for another immediate early IgM-induced gene, *Nr4a1*/NUR77 (Zikherman et al., 2012), and for the self-antigen induced gene *Sdc1*/CD138 (Sabouri et al., 2016). However, EGR2/3 is unique because it not only marks but crucially mediates the IgM-down-regulation response of anergic B cells.

The results here elucidate three key mechanisms of B cell anergy: down-regulation of surface IgM/increased IgD, promotion of germinal centre formation, and inhibition of plasmablast differentiation. IgM^{low} IgD^{high} anergic B cells exhibit ongoing, self-antigen-induced oscillations of intracellular calcium that activate calcineurin to dephosphorylate NFAT for nuclear translocation, while selectively uncoupling IgM/IgD signalling to NF-κB (Healy et al., 1997). However, it was not known if any of the myriad calcium/NFAT activated genes mediate anergy (Glynne et al., 2000). This question is addressed by finding that EGR2/EGR3 deficient B cells not only fail to acquire the IgM^{low} IgD^{high} anergic trait, but one of their most decreased

mRNAs is *Zfp318*, an EGR2-bound gene in CLL that is induced in anergic B cells (Sabouri et al., 2016) and required to promote alternative mRNA splicing of the VDJ_H exon to IgD constant region exons, at the expense of IgM exons (Enders et al., 2014). Consistent with diminished but not absent *Zfp318* mRNA, the increased IgM and lower IgD on EGR2/EGR3-deficient follicular B cells mirrors cells with partial loss-of-function *Zfp318* mutations (Enders et al., 2014). The normal shift to IgD on follicular B cells attenuates IgM signalling to chronic stimulation by self-antigens, and promotes accumulation of IgM^{low} follicular B cells and their recruitment into germinal centre reactions if they bind a foreign antigen (Sabouri et al., 2016).

Three other EGR2 target genes decreased by EGR2/3 deficiency in follicular B cells were *Nfkb2, Il21r* and *Icosl*. IgM^{low} B cells lacking *Nfkb2* have cell autonomously diminished accumulation in follicles (Miosge et al., 2002), while B cells lacking either *Il21r* or *Icosl* are cell autonomously disadvantaged in participating in germinal center reactions (Liu et al., 2015, Tangye and Ma, 2020). EGR2 and EGR3 thus induce a suite of genes that augment follicular B cell recruitment into germinal centre reactions, explaining how this pathway is enhanced in anergic B cells (Sabouri et al., 2016). Promoting germinal centre hypermutation provides a path to remove self-reactivity from immunoglobulins on follicular B cells, by clonal redemption (Burnett et al., 2019).

The third cardinal feature of anergic B cells - their diminished propensity to form plasmablasts (Sabouri et al., 2016), (Goodnow et al., 1989)– is illuminated by finding that EGR2/3-deficient B cells over-expressed a set of EGR2-ChIP-seq target genes normally increased in cells poised for plasma cell differentiation. *Zbtb32* encodes a DNA-binding protein that cooperates with *Prdm1*/BLIMP1 to silence CIITA and is required for long-lived plasma cells (Yoon et al., 2012); *Zbtb20* is an IRF4-induced gene encoding a DNA binding protein that cooperates with *Prdm1*/BLIMP1 to promote plasma cell differentiation and is required for long-lived plasma cells (Chevrier et al., 2014); *Mzb1* is a BLIMP1- and IRF4-

induced gene required for plasma cell accumulation (Andreani et al., 2018). *Il6st* encodes the gp130 signalling subunit of the IL-6 receptor that is required for memory B cells in humans (Schwerd et al., 2017). *Il6ra* encodes the other chain of the IL-6 receptor and *Pim1* encodes an IL-6/STAT3-induced protein kinase required for B cell survival and proliferation (Shirogane et al., 1999). *Lgals1* encodes Galectin-1, which is required for B cell proliferation and plasmablast survival (Tsai et al., 2008). Thus, EGR2 and EGR3 normally repress a suite of key driver genes for pre-plasma cells. They do so not only in follicular B cells, but also in $CD21^{low}$ age-associated and B1 B cells.

The transcriptome of EGR2/3-deficient $CD21^{low}$ $CD23^{low}$ B cells closely resembled that of previously described $CD21^{low}$ B cells. A key question arising from our results is the extent to which deficits in the surface IgM-EGR2/EGR3 pathway contribute to accumulation of $CD21^{low}$ $CD23^{low}$ B cells in human lupus and other autoimmune diseases, or in NZB/W mice. In lupus, these derive in part from activated follicular B cells and contribute to the plasmablast population (Scharer et al., 2019). Inherited mutations or polymorphisms or acquired mutations in *EGR2* itself would likely need to function as dominant negative alleles, given the redundancy demonstrated here between complete null mutations in *Egr2* and *Egr3*. Alternatively, genetic deficits upstream at the level of surface IgM signalling to calcium, calcineurin and NFAT could compromise induction of *EGR2* and *EGR3*.

The dramatic dysregulation of B1 cells in the absence of EGR2 and EGR3 is significant, given that somatic *EGR2* mutations recur in CLL (Damm et al., 2014, Young et al., 2017) and that B1a cells accumulate in autoimmune NZB/W mice (Hayakawa et al., 1983) and mouse models bearing recurrent human CLL mutations (Bichi et al., 2002). Self-reactive transgenic B1 cells can escape clonal deletion by localising to the peritoneal cavity, where they are sequestered from exposure to erythrocyte self-antigens (Okamoto et al., 1992). Mice expressing a transgenic BCR recognising Thy-1 develop Thy-1-specific B1 B cells in the presence – but not

in the absence – of self-antigen (Hayakawa et al., 1999). An inducible switch in BCR specificity of mature B2 cells to express a typical B1 cell BCR, that recognises self-antigen phosphatidylcholine, leads them to proliferate and differentiate into B1 cells (Graf et al., 2019).

Similar to anergic follicular B cells, surface IgM signalling in B1 B cells chronically elevates intracellular calcium and activates NFAT (Wong et al., 2002). The finding here of *Nfatc1* overexpression in CD21^{low} and B1a cells lacking EGR2/EGR3 is notable. In the *Tcl1*-driven mouse model of CLL, deletion of *Nfatc1* in B cells leads to loss of *Egr2* expression and dramatically accelerates accumulation of leukemic CD5^{+} B cells (Marklin et al., 2017). Given that NFATC1 is up-regulated in activated and B1 cells (Healy et al., 1997) and required for B1a cell accumulation and CD5 expression (Berland and Wortis, 2003), our results indicate that *Egr2* and *Egr3* induction by NFATC1 acts as a negative feedback mechanism preventing excessive B1a cell accumulation. Somatic *EGR2* point mutations in the zinc finger domain are more frequent in aggressive CLL (Damm et al., 2014, Young et al., 2017), but it remains unclear to what extent these cause a general loss-of-function, dominant-negative activity that blocks compensation by EGR3, or change the transcriptional specificity of EGR2 as a repressor or activator of the genes defined here.

The results here fill a major gap in understanding tolerance checkpoints mediating B cell anergy and preventing CD21^{low} and B1 B cell accumulation, to prevent autoimmunity. The critical role for EGR2 and EGR3 in anergic, CD21^{low}, and B1 B cells, and the landscape of genes governed by the calcium-NFAT-EGR2/3 checkpoint defined here, will guide future efforts to treat diseases associated with dysregulated accumulation of these cells.

Acknowledgements:

This work was supported by National Health and Medical Research Council (NHMRC) Program (1113904, to C.C.G.) and Fellowship (1081858, to C.C.G.) grants, the UNSW Cellular Genomics Futures Institute, and by The Bill and Patricia Ritchie Foundation. We thank Dr Jonathan D Powell for generously sharing mouse strains, and the Garvan-Weizmann Centre for Cellular Genomics and the Garvan Biological Testing Facility for providing expert technical services.

Author contributions:

E.M-F., J.H.R. and C.C.G. designed the experiments; E.M-F. performed most of the experiments; J.H.R. performed some early experiments; L.A.M., I.A.P provided mouse models used in this study; T.J.P., C.W. and C.C.O conducted RNA-seq and ChIP-Seq bioinformatics analyses; E.M-F., J.H.R. and C.C.G. interpreted the experiments and wrote the manuscript.

FIGURE TITLES AND LEGENDS

Figure 1 –Cell-autonomous accumulation of *Egr2* and *Egr3* deficient CD21^{low} CD23^{low} age-associated-like B cells.

A, Flow cytometric analysis of splenic B220^{pos} CD95^{neg} CD93^{neg} mature CD23^{pos} follicular (FO), CD23^{low} CD21^{pos} marginal zone (MZ) and CD21^{low} CD23^{low} B cells, in *Egr2*$^{+/+}$ *Egr3*$^{+/+}$ (WT) or *Egr2*$^{fl/fl}$ *Egr3*$^{KO/KO}$ (dKO) mice. **B,** Total number per spleen of follicular, marginal zone or CD21^{low} CD23^{low} B cells in *Egr2*$^{+/+}$ *Egr3*$^{+/+}$ (black), *Egr2*$^{fl/fl}$ *Egr3*$^{+/+}$ (yellow), *Egr2*$^{fl/fl}$ *Egr3*$^{KO/+}$ (orange) and *Egr2*$^{fl/fl}$ *Egr3*$^{KO/KO}$ (red) mice. **C,** Number of CD21^{low} CD23^{low} B cells per µL blood, in mice of the indicated genotypes. **D,** *Ptprc, Egr2* and *Egr3* genotypes of bone marrow transplanted into *Rag1*$^{KO/KO}$ mixed to generate chimeric mice. **(E, G, H)** Each circle represents one mouse. Black lines denote cells within one chimeric mouse. **E,** Total number per spleen of *Ptprc*$^{a/a}$ or *Ptprc*$^{b/b}$ B cells, in mixed chimeric mice. **F,** Flow cytometric analysis of CD45.2^{pos} FO, MZ and CD21^{low} CD23^{low} B cells, in mice that received *Egr2*$^{+/+}$ *Egr3*$^{+/+}$ (left) or *Egr2*$^{fl/fl}$ *Egr3*$^{KO/KO}$ (right) *Ptprc*$^{b/b}$ bone marrow. **G,** Total number per spleen of *Ptprc*$^{a/a}$ or *Ptprc*$^{b/b}$ CD21^{low} CD23^{low} B cells, in mixed chimeric mice. **H,** Percentage of *Ptprc*$^{a/a}$ or *Ptprc*$^{b/b}$ mature B

cells with a CD21^{low} CD23^{low} phenotype, in mixed chimeric mice. **(A-H)** Data are represented as mean ± SD. **(A-C)** Data representative of *n* = 3 experiments in mice 8-20 weeks old. Comparisons made by multiple *t*-tests, with Holm-Šidák correction. **(D-H)** Data pooled from *n* > 2 independent experiments with *n* = 4 recipients per group. Comparisons made by paired t-test. * p < 0.05; ** p < 0.01; *** p < 0.001.

Figure 2 – Similarities between CD21^{low} CD23^{low} B cells and *bona fide* age-associated CD21^{low} B cells.

A, Schematic workflow for single-cell RNA sequencing analysis of sorted CD45.1/CD45.2^{+} splenic B1a (CD19^{+} B220^{low} CD5^{+}), CD95^{-} CD93^{-} mature follicular (CD23^{+}) and CD21^{low} CD23^{low} B cells from mixed chimeras transplanted with bone marrow from a *Ptprc*$^{a/a}$ *Egr2*$^{+/+}$ *Egr3*$^{+/+}$ (WT) donor and a *Ptprc*$^{b/b}$ WT or *Egr2*$^{fl/fl}$ *Egr3*$^{KO/KO}$ (dKO) donor. **B,** Unsupervised Uniform Manifold Approximation and Projection (UMAP), following dimensionality reduction of the single-cell RNA short-read sequencing. **C,** Heat map displaying all differentially expressed genes with |log2 fold-change| > 1, between WT (dark blue) and dKO (red) CD21^{low} CD23^{low} (green) and follicular (blue) B cells. **D,** Volcano plot of log2 expression fold-change (log2FC) versus moderated *t*-statistic for differentially expressed genes in CD21^{low} CD23^{low} relative to follicular B cells, irrespective of *Egr2*/*Egr3* genotype, generated using *limma*. **E,** Rank-ordered genes (x axis) and their enrichment scores (y axis) following gene set enrichment analysis (GSEA) of differentially expressed genes in CD21^{low} CD23^{low} relative to follicular B cells, for immunologic terms generated from a published gene set from mouse "age-associated" B cells (Russell Knode et al., 2017).

Figure 3 – Altered gene expression in *Egr2*- and *Egr3*-deficient relative to wild-type CD21^{low} CD23^{low} B cells, including direct EGR2 targets in CLL.

A, Volcano plot of log2 expression fold-change (log2FC) versus moderated *t*-statistic for differentially expressed genes in *Egr2*$^{fl/fl}$ *Egr3*$^{KO/KO}$ (dKO) relative to *Egr2*$^{+/+}$ *Egr3*$^{+/+}$ (WT) CD21^{low} CD23^{low} B cells, generated using *limma*. Black circles denote genes with a FWER < 0.05. **(B, C)** EGR2 chromatin immunoprecipitation sequencing (ChIP-Seq) was performed independently on *n* = 2 samples of human CLL B cells, and these human hg19 genome coordinates were lifted over to mouse mm10 coordinates. **B,** Venn diagrams displaying genes with non-zero expression in ≥1 cell and increased (red) or decreased (blue) expression in dKO relative to WT CD21^{low} CD23^{low} B cells, that also had ≥1 EGR2 ChIP-seq binding site

within 2 kb of their transcription start site (TSS) in ≥1 CLL sample. The enrichment of differentially expressed genes over nearby EGR2 ChIP-seq binding sites was performed using Fisher exact. **C,** Table displaying the top 40 down-regulated (left) or up-regulated (right) genes ranked by |log2FC| in dKO relative to WT $CD21^{low}$ $CD23^{low}$ B cells, that also had ≥1 EGR2 ChIP-Seq binding site within 2 kb of their TSS in human CLL B cells.

Figure 4 – Increased IgM and differential gene expression by *Egr2*- and *Egr3*- deficient follicular B cells.

A, Representative flow cytometric analysis of IgM versus GFP expression by $CD93^{neg}$ $CD23^{pos}$ follicular B cells from an $Egr2^{IRES\text{-}GFP}$ knock-in mouse and an $Egr2^{WT}$ reporter-negative control mouse. Right, slope values following linear regression of IgM versus GFP expression in immature T1, T2/3 and follicular B cells from *n*=4 $Egr2^{IRES\text{-}GFP}$ mice (purple) and *n*=4 $Egr2^{WT}$ reporter-negative mice (grey). Histograms show GFP fluorescence in $Egr2^{IRES\text{-}GFP}$ and $Egr2^{WT}$ cells within the lowest and highest surface IgM quartiles. **(B-F)** $Rag1^{KO/KO}$ mice were transplanted with a 1:1 mixture of $Ptprc^{a/a}$ $Egr2^{+/+}$ $Egr3^{+/+}$ (WT, black) and $Ptprc^{b/b}$ $Egr2^{+/+}$ $Egr3^{+/+}$ (WT, blue) or $Egr2^{fl/fl}$ $Egr3^{KO/KO}$ (dKO, red) bone marrow. Data representative of *n*=3 experiments with *n*>4 mice per group. **B,** Flow cytometric analysis of IgM versus IgD expression on $Ptprc^{a/a}$ WT (black) versus $Ptprc^{b/b}$ WT (blue) or dKO (red) mature B cell populations. **C,** Histogram overlays of IgM and IgD expression on $Ptprc^{a/a}$ WT (black) versus $Ptprc^{b/b}$ dKO (red) follicular B cells. **D,** Volcano plot of log2 expression fold-change versus moderated *t*-statistic for differentially expressed genes in dKO relative to WT follicular B cells. Red circles denote genes with a FWER<0.05. **(E,F)** EGR2 chromatin immunoprecipitation sequencing (ChIP-Seq) was performed independently on *n*=2 CLL, and human hg19 lifted over to mouse mm10 genome coordinates. **E,** Overlap of genes with increased (red) or decreased (blue) expression in dKO versus WT follicular B cells, that also had ≥1 EGR2 ChIP-seq binding site within 2 kb of their transcription start site (TSS), in ≥1 CLL sample. **F,** Top 24 down- (left) or up-regulated (right) genes, ranked by |log2FC| in dKO versus WT follicular B cells, with ≥1 EGR2 ChIP-Seq binding site <2 kb of their TSS in CLL.

Figure 5 - *Egr2*- and *Egr3*-deficiency causes the cell-autonomous accumulation of B1 cells.

A, Flow cytometric analysis of $CD19^{pos}$ $CD23^{neg}$ $CD5^{pos}$ B1a, $CD23^{neg}$ $CD5^{neg}$ B1b and $CD23^{pos}$ $CD5^{neg}$ B2 cells in $Egr2^{+/+}$ $Egr3^{+/+}$ (WT) and $Egr2^{fl/fl}$ $Egr3^{KO/KO}$ (dKO) mice (left) and their total

numbers in the peritoneal cavity of *Egr2*$^{+/+}$ *Egr3*$^{+/+}$ (black), *Egr2*$^{fl/fl}$ *Egr3*$^{+/+}$ (yellow), *Egr2*$^{fl/fl}$ *Egr3*$^{KO/+}$ (orange) and *Egr2*$^{fl/fl}$ *Egr3*$^{KO/KO}$ (red) mice (right). **B,** Total number of CD19^{pos} B220^{int} CD23^{low} CD5^{pos} CD43^{high} B1a cells per spleen (left), femur bone (middle) or µL of blood (left), in mice of the indicated genotypes. **(C-E)** *Rag1*$^{KO/KO}$ mice were transplanted with a 1:1 mixture of bone marrow from a *Ptprc*$^{a/a}$ *Egr2*$^{+/+}$ *Egr3*$^{+/+}$ donor and from a *Ptprc*$^{b/b}$ donor lacking neither, one or both alleles of *Egr2* and/or *Egr3*. Lines link cells within individual chimeric mice. **C,** Flow cytometric analysis of CD45.1^{+} (top) or CD45.2^{+} (bottom) B1a, B1b and B2 cells in the peritoneal cavity of chimeras that received *Ptprc*$^{b/b}$ dKO bone marrow. **D,** Total number of *Ptprc*$^{a/a}$ or *Ptprc*$^{b/b}$ B1a, B1b or B2 cells in the peritoneal cavity of mice that received bone marrow of the indicated genotypes. **E,** Total number of *Ptprc*$^{a/a}$ or *Ptprc*$^{b/b}$ B1a cells per spleen (left) or per µL of blood (right), in mice that received bone marrow of the indicated genotypes. **(A-E)** Data are represented as mean ± SD. **(A,B)** Data representative of n=3 experiments in mice 8-20 weeks old. Comparisons made by multiple t-tests with Holm-Šidák correction. **(C-E)** Data pooled from n=2 independent experiments with n=4 recipients per group. Comparisons within a chimeric mouse made by paired t-test. * $p < 0.05$; ** $p < 0.01$; *** $p < 0.001$.

Figure 6 – Shared differential gene expression, including of EGR2 targets in CLL, by *Egr2*- and *Egr3*-deficient B1a and CD21^{low} B cells relative to controls.

(**A-C**) Single-cell RNA sequence analysis was performed on CD45.1/CD45.2^{+} B1a cells as for other splenic subsets in Figures 2-4. **A,** Overlap of genes significantly (FWER < 0.05) increased (log2FC>0.3) or decreased (log2FC<-0.3) in dKO relative to WT cells, for both CD21^{low} CD23^{low} (green) and B1a (purple) cells. **B,** Overlap of genes significantly (FWER < 0.05) increased (log2FC>0) or decreased (log2FC<0) in dKO relative to WT B1a cells, with genes with non-zero expression and ≥1 EGR2 ChIP-Seq binding site within 2 kb of their transcription start site (TSS) in ≥1 CLL sample. **C,** Scatter plot of genes with EGR2 binding sites within 2 kb of their TSS that were also within the top 200 most differentially expressed genes in dKO versus WT cells, for both B1a and CD21^{low} CD23^{low} B cells.

METHODS

Mouse handling

All mouse handling and experimental methods were performed in accordance with approved protocols of the Garvan Institute of Medical Research/St Vincent's Hospital Animal Ethics Committee. All mice were bred and maintained in specific pathogen-free conditions at Australian BioResources (ABR; Moss Vale, Australia) or at the Garvan Institute of Medical Research Biological Testing Facility (BTF). All experiments conformed to the current guidelines from the Australian Code of Practice for the Care and Use of Animals for Scientific Purposes. Mice were genotyped by the Garvan Molecular Genetics (GMG) facility at the Garvan Institute of Medical Research.

Mouse strains

Cd19^{Cre} mice (Rickert et al., 1997) were obtained from the Jackson laboratory, Bar Harbor, ME. *Egr2* floxed (*Egr2*^{fl}) (Taillebourg et al., 2002) and *Egr3* knockout (*Egr3*^{KO}) mice (Tourtellotte and Milbrandt, 1998) were generously provided by Dr. Jonathan D Powell. They were back-crossed >10 generations onto a C57BL/6Ncrl background and crossed with *Cd19*^{Cre} mice. *Egr2*-IRES-GFP reporter mice (Williams et al., 2017) were used to compare *Egr2* and surface IgM expression. These mice express an internal ribosome entry sequence (IRES) followed by the coding region of green fluorescent protein (GFP) targeted into the 3' untranslated region of the *Egr2* gene (Williams et al., 2017).

C57BL/6 JAusb (C57BL/6J), C57BL/6 NCrl, B6.JSL-*Ptprc*^{a}*Pepc*^{b} (CD45.1) and B6.129S7-*Rag1*^{tm1Mom}/J (*Rag1*$^{KO/KO}$) mice were purchased from ABR.

Chimeras

To generate 100% chimeras, age- and sex-matched *Rag1*$^{KO/KO}$ mice were irradiated with one dose of 425 Rad from an X-ray source (X-RAD 320 Biological Irradiator, PXI). Recipient mice

were then injected with donor bone marrow from *Egr2*^{fl} *Egr3*^{KO} mice lacking one or both alleles of *Egr2* and/or *Egr3*.

To generate mixed chimeras, age- and sex-matched *Rag1*$^{KO/KO}$ mice were irradiated with one dose of 425 Rad and 12 hours later, injected with a 1:1 mixture of *Ptprc*$^{a/a}$ bone marrow from B6.JSL-*Ptprc*^{a}*Pepc*^{b} donor mice and of *Ptprc*$^{b/b}$ cells from *Egr2*^{fl} *Egr3*^{KO} donor mice lacking one or both alleles of *Egr2* and/or *Egr3*. The bone marrow cell suspension was depleted of lineage-positive cells (expressing B220, CD3, CD4, CD8, CD11b, CD11c, CD19, LY-6C, LY-6G, NK1.1, TCRβ) prior to injection. Each recipient mouse received 2-6 x 10^6 donor bone marrow cells injected intravenously.

Flow cytometry and cell-sorting.

Single-cell suspensions were prepared from mouse spleen, bone marrow, inguinal lymph nodes, peritoneal cavity and blood. 1-4 x 10^6 cells in PBS 2% FCS were transferred into appropriate wells of a 96-well U bottom plate. To prevent non-specific antibody binding, cells were incubated with F_c blocking antibody for 20 min at 4°C in the dark. Cells were then incubated with antibodies for 30 min, on ice and in the dark. To fix cells, they were incubated in 10% formalin (Sigma-Aldrich) for 15 min at 4°C, and washed and resuspended in PBS 2% FCS. To stain for intracellular nuclear proteins, cells were fixed and permeabilised using the manufacturer's instructions and the eBioscience Transcription Factor Staining kit. Stained single-cell suspensions were acquired on the BD LSRFortessa™. To determine total numbers of populations in the peritoneal cavity, the totality of harvested cells from the peritoneal cavity wash were acquired on the BD LSRFortessa™.

Where appropriate, following extracellular antibody staining, immune populations were sorted by fluorescence-activated cell sorting (FACS) on a FACS Aria III (BD Biosciences).

567 **Anti-mouse antibodies used for flow cytometric analyses.**

Cat number	Antibody/dye	Fluorochrome	Company	Clone
A1310	7AAD	N/A	Invitrogen	N/A
17-0051-81	CD5	APC	Thermo Fischer	53-7.3
557396	CD11b	FITC	BioLegend	M1/70
101208	CD11b	PE	BioLegend	M1/70
45-0114-82	CD11c	PerCP/Cy5.5	eBioscience	N418
115546	CD19	BV510	BioLegend	6D5
115539	CD19	BV605	BioLegend	6D5
553818	CD21/35	FITC	BD Biosciences	7G6
101614	CD23	PE/Cy7	BioLegend	B3B4
101820	CD24	Pacific Blue	BD Biosciences	M1/69
562768	CD38	BV421	BD Biosciences	Ab90
553270	CD43	FITC	BD Biosciences	S7
564574	CD45.1	BUV737	BD Biosciences	A20
110716		APC Cy7	Biolegend	A20
110728		PerCP Cy5.5	Biolegend	A20
560696	CD45.2	PE Cy7	BD Biosciences	104
564616		BUV395	BD Biosciences	104
109824		APC Cy7	BioLegend	104

564449	CD45R/B220	BUV737	BD Biosciences	RA3-6B2
740877	CD86	BV786	BD Biosciences	GL1
17-5892-83	CD93	APC	eBioscience	AA4.1
557653	CD95	PE Cy7	BD Biosciences	Jo2
565988	IgD	BUV395	BD Biosciences	11-26c.2a
559750	Ig, κ light chain	Biotin	BD Biosciences	187.1
407308	Ig, λ light chain	PE	BioLegend	RML-42
406515	IgM	APC/Cy7	BioLegend	RMM-1
405229	Streptavidin	BV605	BioLegend	N/A
644814	T-bet	APC	BioLegend	4B10

Chromatin Immunoprecipitation sequencing (ChIP-Seq)

ChIP-seq was carried out using 30 µg of chromatin isolated from cryopreserved PBMC samples obtained from two CLL patients and 4 µl of anti-EGR2 antibody (Abcam, cat# ab43020, Lot# GR101477-1). The immunoprecipitated DNA was processed into a standard Illumina ChIP-seq library and sequenced on an Illumina HiSeq instrument (Illumina) generating 48 and 35 million 75-nt single-end (SE75) sequence reads. Chromatin was pooled from both samples to generate the input control sequencing library. Sequence reads were mapped to the genome (hg38) using the BWA algorithm with default settings following standard Illumina purity filtering, duplicate read removal, unique mapping, and allowing ≤2 mismatches, generating 28 and 18 million sequence tags. Normalization was performed by down-sampling the number of tags to the lowest number between samples (18 million). Peak intervals were called using the MACS (Zhang et al., 2008) algorithm with the default cut-off *p*

value 10^{-7}. Peak filtering was performed by removing false ChIP-seq peaks as defined within the ENCODE blacklist.

Single-cell RNA sequencing using the 10X platform

To assess the cell-autonomous effects of *Egr2* and *Egr3* deficiency on gene expression in B cells, we sorted CD45.1$^+$ *Egr2*$^{+/+}$ *Egr3*$^{+/+}$ (WT) or CD45.2$^+$ *Egr2*$^{fl/fl}$ *Egr3*$^{KO/KO}$ (dKO) splenic mature follicular, CD21^{low} CD23^{low} and B1a cells from *n* = 4 "test" chimeras. To control for any effects of *Ptprc*$^{a/a}$ (CD45.1) versus *Ptprc*$^{b/b}$ (CD45.2) expression, we sorted CD45.1$^+$ WT and CD45.2$^+$ WT cells from *n* = 1 control chimera, and later corrected differential gene expression for any differences observed in this comparison at the modelling stage.

Mouse B cells were bulk sorted from mixed chimeras into Eppendorf tubes containing cold sterile PBS 10% FCS and incubated for 20 min at 4°C with TotalSeq™ DNA-barcoded anti-mouse 'Hashing' antibodies (BioLegend) at a 1/100 final dilution. The TotalSeq™ antibodies contain a mixture of two monoclonal antibodies, both conjugated to the same DNA oligonucleotide, that are specific against mouse CD45 and MHC class I haplotypes – and thus stain all leukocytes from C57BL/6 mice.

During the incubation, cells were transferred into a 96-well round bottom plate, on ice. Following incubation, cells were washed three times in cold PBS 2% FCS and the hashed populations pooled into mixtures for single-cell RNA sequencing using the 10X Genomics platform. The Garvan-Weizmann Centre for Cellular Genomics (GWCCG) performed the 10X capture, and sequencing of resulting cDNA samples, as an in-house commercial service, using the Chromium Single-Cell v2 3' Kits (10X Genomics). A total of 5,000 to 12,000 cells were captured per reaction.

RNA libraries were sequenced on an Illumina NovaSeq 6000 (NovaSeq Control Software v 1.6.0 / Real Time Analysis v3.4.4) using a NovaSeq S4 230 cycles kit (Illumina, 20447086) as

follows: 28bp (Read 1), 91bp (Read 2) and 8bp (Index). HASHing libraries were sequenced on an Illumina NextSeq 500/550 (NextSeq Control Software v 2.2.0.4 / Real Time Analysis 2.4.11) using a NextSeq 60 cycles kit (Illumina, 20456719) as follows: 28bp (Read 1), 24bp (Read 2) and 8bp (Index). Sequencing generated raw data files in binary base call (BCL) format. These files were demultiplexed and converted to FASTQ using Illumina Conversion Software (bcl2fastq v2.19.0.316). Alignment, filtering, barcode counting and UMI counting were performed using the Cell Ranger Single Cell Software v3.1.0 (10X Genomics). Reads were aligned to the mm10-3.0.0 (release 84) mouse reference genomes. Raw count matrices were exported and filtered using the EmptyDrops package in R (Lun et al., 2019).

DNA-barcoded anti-mouse Hashing antibodies.

Cat number	Name	Clones	Barcode
155801	TotalSeq™-A0301 anti-mouse Hashtag 1 Antibody	M1/42; 30-F11	ACCCACCAGTAAGAC
155803	TotalSeq™-A0302 anti-mouse Hashtag 2 Antibody	M1/42; 30-F11	GGTCGAGAGCATTCA
155813	TotalSeq™-A0307 anti-mouse Hashtag 7 Antibody	M1/42; 30-F11	GAGTCTGCCAGTATC
155815	TotalSeq™-A0308 anti-mouse Hashtag 8 Antibody	M1/42; 30-F11	TATAGAACGCCAGGC
155817	TotalSeq™-A0309 anti-mouse Hashtag 9 Antibody	M1/42; 30-F11	TGCCTATGAAACAAG

155819	TotalSeq™-A0310 anti-mouse Hashtag 10 Antibody	M1/42; 30-F11	CCGATTGTAACAGAC
155821	TotalSeq™-A0311 anti-mouse Hashtag 11 Antibody	M1/42; 30-F11	GCTTACCGAATTAAC
155823	TotalSeq™-A0312 anti-mouse Hashtag 12 Antibody	M1/42; 30-F11	CTGCAAATATAACGG

Statistical analyses.

Statistical analyses of flow cytometric experiments were performed using the GraphPad Prism 6 software (GraphPad, San Diego, USA). A one-tailed unpaired Student's *t*-test with Welch's correction was used for comparisons between two normally distributed groups. An unpaired student's *t*-test, corrected for multiple comparisons using the Holm-Sidak method, was used for comparisons of more than two groups. Differences between paired measurements were analysed by paired *t*-test. In all graphs presented, the error bars represent the mean and standard deviation. * $p < 0.05$, ** $p < 0.01$, *** $p < 0.001$.

For the 10X analysis, cells were excluded if the library size or number of expressed genes fell below 2 median absolute deviations, or if mitochondrial reads accounted for more than 20% of total reads. Cell-wise gene expression counts were normalized and recovered using SAVER (Huang et al., 2018) with default values, and differentially expressed genes (DEGs) were identified using limma (Ritchie et al., 2015) on the log-transformed recovered counts. Where appropriate, fold changes and *p*-values were reported after correcting for the *Ptprc* genotype effect during the linear modelling process, through a set of post-hoc contrasts. Bonferroni correction was applied to each set of *p*-values. DEGs were defined as having a family-wise error rate (FWER) < 0.05.

For the EGR2 ChIP-seq analysis, the human genome coordinates of EGR2-bound genes were lifted over to mm10 and a distance below 2 kb from the transcription start site (TSS) was used to define EGR2 peaks in proximity to a given gene. Significant enrichment of differentially expressed (FWER < 0.05) EGR2 target genes identified in at least one independent ChIP-Seq experiment was calculated using a Fisher exact test.

SUPPLEMENTAL INFORMATION TITLES AND LEGENDS

Supplementary Figure 1 – No changes in bone marrow B cell populations but increased numbers of splenic immature T1 B cells in *Egr2*- and *Egr3*-deficient mice.

A, Representative flow cytometric analysis of $B220^{pos}$ B cells, IgM^{neg} IgD^{neg} precursor ($CD43^{pos}$ $CD24^{neg}$ pre-pro-, $CD43^{int}$ $CD24^{int}$ pro- and $CD43^{low}$ $CD24^{pos}$ pre-B), IgM^{pos} IgD^{int} immature ($CD23^{neg}$ T1 and $CD23^{pos}$ T2) and IgM^{low} IgD^{high} mature recirculating B cells in the bone marrow of $Egr2^{+/+}$ $Egr3^{+/+}$ (top) or $Egr2^{fl/fl}$ $Egr3^{KO/KO}$ (bottom) mice. **B,** Percentage of parent population (top) or total number per femur (bottom) of bone marrow B cell populations in $Egr2^{+/+}$ $Egr3^{+/+}$ (black), $Egr2^{fl/fl}$ $Egr3^{+/+}$ (yellow), $Egr2^{fl/fl}$ $Egr3^{KO/+}$ (orange) and $Egr2^{fl/fl}$ $Egr3^{KO/KO}$ (red) mice. **C,** Percentage of parent population (top) or total number per spleen (bottom) of splenic $B220^{pos}$ B cells (left), $CD93^{pos}$ immature versus $CD93^{neg}$ mature (middle) and immature $CD23^{neg}$ T1, $CD23^{pos}$ IgM^{high} T2 and $CD23^{pos}$ IgM^{low} T3 (right), in mice of the indicated genotypes. **D,** Representative flow cytometric analysis of splenic immature B cell populations, in $Egr2^{+/+}$ $Egr3^{+/+}$ (top) or $Egr2^{fl/fl}$ $Egr3^{KO/KO}$ (bottom) mice. (**B,C**) Data are represented as mean ± SD. Data are representative of $n = 3$ experiments in mice 8-20 weeks old. Comparisons made by multiple *t*-tests with Holm-Šidák correction. * $p < 0.05$; ** $p < 0.01$; *** $p < 0.001$.

Supplementary Figure 2 – Reduced B cell CD21 and CD23 expression and accumulation of $CD21^{low}$ $CD23^{low}$ B cells in the bone marrow of *Egr2*- and *Egr3*-deficient mice.

A, Left, representative flow cytometric analysis of mature recirculating bone marrow B cell populations, based on CD21 and CD23 cell-surface expression. Right, percentage of $CD21^{low}$ $CD23^{low}$ B cells within mature recirculating B cells in the bone marrow of $Egr2^{+/+}$ $Egr3^{+/+}$ (black), $Egr2^{fl/fl}$ $Egr3^{+/+}$ (yellow), $Egr2^{fl/fl}$ $Egr3^{KO/+}$ (orange) and $Egr2^{fl/fl}$ $Egr3^{KO/KO}$ (red) mice.

B, Mean fluorescence intensity (MFI) of cell-surface antibody staining for CD21 (top) or CD23 (bottom) on bone marrow and splenic B cell populations in mice of the indicated genotypes. (**A,B**) Data are represented as mean ± SD. Data are representative of *n* = 3 experiments in mice 8-20 weeks old. Comparisons made by multiple *t*-tests with Holm-Šidák correction. * $p < 0.05$; ** $p < 0.01$; *** $p < 0.001$.

Supplementary Figure 3 – Accumulation of splenic CD21^{low} CD23^{low} B cells in mice transplanted with *Egr2$^{fl/fl}$ Egr3$^{KO/KO}$* bone marrow.

(**A,B**) *Rag1$^{KO/KO}$* mice were irradiated and transplanted with bone marrow cells from a *Ptprc$^{b/b}$* donor mouse that was *Egr2$^{fl/+}$ Egr3$^{+/+}$* (black) or *Egr2$^{fl/+}$ Egr3$^{KO/+}$* (light orange) or *Egr2$^{fl/fl}$ Egr3$^{KO/KO}$* (red). **A,** Frequency of CD19^{pos} B cells, CD93^{pos} immature versus CD93^{neg} mature and of CD23^{neg} T1, CD23^{pos} IgM^{high} T2 and CD23^{pos} IgM^{low} T3 immature B cells, as percentage of splenic leukocytes, in mice transplanted with bone marrow cells of the indicated genotypes. **B,** Left, representative flow cytometric analysis of B220^{pos} CD95^{neg} CD93^{neg} mature B cells with a CD23^{pos} follicular, CD23^{low} CD21^{pos} marginal zone or CD21^{low} CD23^{low} B cells phenotype, in *Egr2$^{+/+}$ Egr3$^{+/+}$* (top) or *Egr2$^{fl/fl}$ Egr3$^{KO/KO}$* (bottom) mice. Right, percentage of mature B cells or total number per spleen of follicular, marginal zone and CD21^{low} B cells in mice of the indicated genotypes. (**A,B**) Data are represented as mean ± SD. Data representative of *n* = 1 experiment, with *n* = 7 mice per group. Comparisons made by multiple *t*-tests with Holm-Šidák correction. * $p < 0.05$; ** $p < 0.01$; *** $p < 0.001$.

Supplementary Figure 4 – Schematic workflow and principle components analysis of single-cell RNA sequencing of splenic B cell populations from mixed chimeras.

A, *Rag1$^{KO/KO}$* mice were transplanted with a 1:1 mixture of bone marrow from a *Ptprc$^{a/a}$ Egr2$^{+/+}$ Egr3$^{+/+}$* (WT) donor and from an *Egr$^{+/+}$ Egr3$^{+/+}$* (WT) or *Egr2$^{fl/fl}$ Egr3$^{KO/KO}$* (dKO) *Ptprc$^{b/b}$* donor. Following reconstitution, CD45.1/CD45.2^{+} splenic CD19^{pos} B220^{int} CD5^{pos} CD23^{low} B1a cells, CD19^{pos} B220^{pos} CD95^{neg} CD93^{neg} mature CD23^{pos} follicular or CD21^{low} CD23^{low} B cells were bulk-sorted from 1 "control" chimera that received WT *Ptprc$^{b/b}$* bone marrow and from 4 "test" chimeras that received dKO *Ptprc$^{b/b}$* bone marrow. Each purified population was incubated with a uniquely DNA-barcoded TotalSeq™ Hashtag antibody and the barcoded populations were pooled for single-cell RNA sequencing using the Chromium 3' 10X platform. **B,** Unsupervised analysis using principal components analysis (PCA) of 'pseudobulk' gene expression levels in DNA-barcoded populations: B1a cells (squares),

mature follicular (circles) and CD21^{low} CD23^{low} (triangles) B cells that were *Ptprc*$^{a/a}$ WT (dark blue fill) or *Ptprc*^{bb} WT (light blue fill) or *Ptprc*$^{b/b}$ dKO (red fill). **C,** Rank-ordered genes (x axis) and their enrichment scores (y axis) following gene set enrichment analysis (GSEA) of differentially expressed genes in CD21^{low} CD23^{low} relative to follicular B cells, for immunologic terms generated from a published gene set from mouse "CD11c^{+}" B cells (Rubtsov et al., 2011).

Supplementary Figure 5 – Negative correlation of cell-surface IgM and *Egr2* gene expression in an *Egr2*-IRES-GFP mouse model.

A, Representative gating and linear regression of cell-surface IgM expression on CD23^{neg} CD93^{pos} immature T1 (left) or CD23^{pos} CD93^{pos} T2/T3 (right) B cells versus green fluorescent protein (GFP) fluorescence, in *Egr2*-IRES-GFP reporter mice. **B,** Representative histogram overlays of GFP expression by T1, T2/T3 or CD93^{neg} CD23^{pos} follicular B cells from *Egr2*$^{IRES\text{-}GFP}$ mice, gated on cells in the lowest quartile (blue) and highest quartile (red) for cell-surface IgM expression. **C,** Representative histogram overlays of GFP expression by T1, T2/T3 or follicular B cells in the highest (top) or lowest (bottom) quartiles for cell-surface IgM expression, from *Egr2*$^{IRES\text{-}GFP}$ reporter mice (purple) relative to *Egr2*^{WT} reporter negative control mice (black). Data representative of *n*=4 mice per group.

Supplementary Figure 6 – Altered cell-surface IgM and IgD and *Zfp318* gene expression in *Egr2*- and *Egr3*-deficient B cells.

(**A-C**) *Rag1*$^{KO/KO}$ mice were transplanted with a 1:1 mixture of bone marrow from a *Ptprc*$^{a/a}$ *Egr2*$^{+/+}$ *Egr3*$^{+/+}$ donor and from a *Ptprc*$^{b/b}$ donor lacking neither, one or both alleles of *Egr2* and/or *Egr3*. **A,** Mean fluorescence intensity of cell-surface IgM (left) and IgD (right) expression following flow cytometric analysis of B220^{+} CD19^{+} CD95^{-} CD93^{-} CD23^{+} follicular B cells from mixed chimeras that received bone marrow of the indicated genotypes. Data are represented as mean ± SD. Comparisons within individual chimeric mice were made by paired *t*-test. * $p < 0.05$; ** $p < 0.01$; *** $p < 0.001$. **B,** Violin plots showing kernel density estimations of *Zfp318* gene expression, at single-cell resolution, following single-cell RNA sequencing analysis of *Egr2*$^{fl/fl}$ *Egr3*$^{KO/KO}$ (dKO; red fill) and *Egr2*$^{+/+}$ *Egr3*$^{+/+}$ (WT; grey) mature follicular and CD21^{low} CD23^{low} B cells from mixed chimeras. **C,** Representative histogram overlays for IgM (top) or IgD (bottom) cell-surface expression on *Ptprc*$^{a/a}$ WT (black line) versus *Ptprc*$^{b/b}$

dKO (red fill) splenic B cell populations from chimeric mice. Data representative of $n > 2$ independent experiments with $n > 4$ mice per group.

SUPPLEMENTARY TABLE TITLES

Supplementary Table 1: Gene set enrichment analysis in $CD21^{low}$ $CD23^{low}$ relative to follicular B cell differentially expressed genes, for genes up-regulated in $B220^{+}$ $CD93^{-}$ $CD43^{-}$ $CD21^{-}$ $CD23^{-}$ relative to follicular B cells (GSE81650).

Supplementary Table 2: Gene set enrichment analysis in $CD21^{low}$ $CD23^{low}$ relative to follicular B cell differentially expressed genes, for genes down-regulated in $B220^{+}$ $CD93^{-}$ $CD43^{-}$ $CD21^{-}$ $CD23^{-}$ relative to follicular B cells (GSE81650).

Supplementary Table 3: Genes up-regulated in *Egr2/3* dKO relative to WT $CD21^{low}$ B cells.

Supplementary Table 4: Genes down-regulated in *Egr2/3* dKO relative to WT $CD21^{low}$ B cells.

Supplementary Table 5: Genes differentially expressed in *Egr2/3* dKO relative to WT $CD21^{low}$ B cells, with at least one EGR2 ChIP-Seq peak within 2kb from their transcription start site.

Supplementary Table 6: Genes up-regulated in *Egr2/3* dKO relative to WT follicular B cells.

Supplementary Table 7: Genes down-regulated in *Egr2/3* dKO relative to WT follicular B cells.

Supplementary Table 8: Genes differentially expressed in *Egr2/3* dKO relative to WT follicular B cells, with at least one EGR2 ChIP-Seq peak within 2kb from their transcription start site.

Supplementary Table 9: Genes up-regulated in *Egr2/3* dKO relative to WT B1a B cells.

Supplementary Table 10: Genes down-regulated in *Egr2/3* dKO relative to WT B1a B cells.

Supplementary Table 11: Genes differentially expressed in *Egr2/3* dKO relative to WT B1a B cells, with at least one EGR2 ChIP-Seq peak within 2kb from their transcription start site.

REFERENCES

ANDREANI, V., RAMAMOORTHY, S., PANDEY, A., LUPAR, E., NUTT, S. L., LAMMERMANN, T. & GROSSCHEDL, R. 2018. Cochaperone Mzb1 is a key effector of Blimp1 in plasma cell differentiation and beta1-integrin function. *Proc Natl Acad Sci U S A,* 115**,** E9630-E9639.

APOLLONIO, B., SCIELZO, C., BERTILACCIO, M. T., TEN HACKEN, E., SCARFO, L., RANGHETTI, P., STEVENSON, F., PACKHAM, G., GHIA, P., MUZIO, M. & CALIGARIS-CAPPIO, F. 2013. Targeting B-cell anergy in chronic lymphocytic leukemia. *Blood,* 121**,** 3879-88, S1-8.

BENEDETTO, A., DI CARO, A., CAMPORIONDO, M. P., GALLONE, D., ZANIRATTI, S., TOZZI, V. & ELIA, G. 1992. Identification of a CD21 receptor-deficient, non-Ig-secreting peripheral B lymphocyte subset in HIV-seropositive drug abusers. *Clin Immunol Immunopathol,* 62**,** 139-47.

BERLAND, R. & WORTIS, H. H. 2003. Normal B-1a cell development requires B cell-intrinsic NFATc1 activity. *Proc Natl Acad Sci U S A,* 100**,** 13459-64.

BICHI, R., SHINTON, S. A., MARTIN, E. S., KOVAL, A., CALIN, G. A., CESARI, R., RUSSO, G., HARDY, R. R. & CROCE, C. M. 2002. Human chronic lymphocytic leukemia modeled in mouse by targeted TCL1 expression. *Proc Natl Acad Sci U S A,* 99**,** 6955-60.

BURNETT, D. L., REED, J. H., CHRIST, D. & GOODNOW, C. C. 2019. Clonal redemption and clonal anergy as mechanisms to balance B cell tolerance and immunity. *Immunol Rev,* 292**,** 61-75.

CHARLES, E. D., BRUNETTI, C., MARUKIAN, S., RITOLA, K. D., TALAL, A. H., MARKS, K., JACOBSON, I. M., RICE, C. M. & DUSTIN, L. B. 2011. Clonal B cells in patients with hepatitis C virus-associated mixed cryoglobulinemia contain an expanded anergic CD21low B-cell subset. *Blood,* 117**,** 5425-37.

CHEVRIER, S., EMSLIE, D., SHI, W., KRATINA, T., WELLARD, C., KARNOWSKI, A., ERIKCI, E., SMYTH, G. K., CHOWDHURY, K., TARLINTON, D. & CORCORAN, L. M. 2014. The BTB-ZF transcription factor Zbtb20 is driven by Irf4 to promote plasma cell differentiation and longevity. *J Exp Med,* 211**,** 827-40.

DAMM, F., MYLONAS, E., COSSON, A., YOSHIDA, K., DELLA VALLE, V., MOULY, E., DIOP, M., SCOURZIC, L., SHIRAISHI, Y., CHIBA, K., TANAKA, H., MIYANO, S., KIKUSHIGE, Y., DAVI, F., LAMBERT, J., GAUTHERET, D., MERLE-BERAL, H., SUTTON, L., DESSEN, P., SOLARY, E., AKASHI, K., VAINCHENKER, W., MERCHER, T., DROIN, N., OGAWA, S., NGUYEN-KHAC, F. & BERNARD, O. A. 2014. Acquired initiating mutations in early hematopoietic cells of CLL patients. *Cancer Discov,* 4**,** 1088-101.

DUTY, J. A., SZODORAY, P., ZHENG, N. Y., KOELSCH, K. A., ZHANG, Q., SWIATKOWSKI, M., MATHIAS, M., GARMAN, L., HELMS, C., NAKKEN, B., SMITH, K., FARRIS, A. D. & WILSON, P. C. 2009. Functional anergy in a subpopulation of naive B cells from healthy humans that express autoreactive immunoglobulin receptors. *J Exp Med,* 206**,** 139-51.

ENDERS, A., SHORT, A., MIOSGE, L. A., BERGMANN, H., SONTANI, Y., BERTRAM, E. M., WHITTLE, B., BALAKISHNAN, B., YOSHIDA, K., SJOLLEMA, G., FIELD, M. A., ANDREWS, T. D., HAGIWARA, H. & GOODNOW, C. C. 2014. Zinc-finger protein ZFP318 is essential

for expression of IgD, the alternatively spliced Igh product made by mature B lymphocytes. *Proc Natl Acad Sci U S A,* 111**,** 4513-8.

GLYNNE, R., AKKARAJU, S., HEALY, J. I., RAYNER, J., GOODNOW, C. C. & MACK, D. H. 2000. How self-tolerance and the immunosuppressive drug FK506 prevent B-cell mitogenesis. *Nature,* 403**,** 672-6.

GOODNOW, C. C., CROSBIE, J., JORGENSEN, H., BRINK, R. A. & BASTEN, A. 1989. Induction of self-tolerance in mature peripheral B lymphocytes. *Nature,* 342**,** 385-91.

GRAF, R., SEAGAL, J., OTIPOBY, K. L., LAM, K. P., AYOUB, S., ZHANG, B., SANDER, S., CHU, V. T. & RAJEWSKY, K. 2019. BCR-dependent lineage plasticity in mature B cells. *Science,* 363**,** 748-753.

HAO, Y., O'NEILL, P., NARADIKIAN, M. S., SCHOLZ, J. L. & CANCRO, M. P. 2011. A B-cell subset uniquely responsive to innate stimuli accumulates in aged mice. *Blood,* 118**,** 1294-304.

HAYAKAWA, K., ASANO, M., SHINTON, S. A., GUI, M., ALLMAN, D., STEWART, C. L., SILVER, J. & HARDY, R. R. 1999. Positive selection of natural autoreactive B cells. *Science,* 285**,** 113-6.

HAYAKAWA, K., HARDY, R. R., PARKS, D. R. & HERZENBERG, L. A. 1983. The "Ly-1 B" cell subpopulation in normal immunodefective, and autoimmune mice. *J Exp Med,* 157**,** 202-18.

HEALY, J. I., DOLMETSCH, R. E., TIMMERMAN, L. A., CYSTER, J. G., THOMAS, M. L., CRABTREE, G. R., LEWIS, R. S. & GOODNOW, C. C. 1997. Different nuclear signals are activated by the B cell receptor during positive versus negative signaling. *Immunity,* 6**,** 419-28.

HUANG, M., WANG, J., TORRE, E., DUECK, H., SHAFFER, S., BONASIO, R., MURRAY, J. I., RAJ, A., LI, M. & ZHANG, N. R. 2018. SAVER: gene expression recovery for single-cell RNA sequencing. *Nat Methods,* 15**,** 539-542.

ISNARDI, I., NG, Y. S., MENARD, L., MEYERS, G., SAADOUN, D., SRDANOVIC, I., SAMUELS, J., BERMAN, J., BUCKNER, J. H., CUNNINGHAM-RUNDLES, C. & MEFFRE, E. 2010. Complement receptor 2/CD21- human naive B cells contain mostly autoreactive unresponsive clones. *Blood,* 115**,** 5026-36.

JENKS, S. A., CASHMAN, K. S., ZUMAQUERO, E., MARIGORTA, U. M., PATEL, A. V., WANG, X., TOMAR, D., WOODRUFF, M. C., SIMON, Z., BUGROVSKY, R., BLALOCK, E. L., SCHARER, C. D., TIPTON, C. M., WEI, C., LIM, S. S., PETRI, M., NIEWOLD, T. B., ANOLIK, J. H., GIBSON, G., LEE, F. E., BOSS, J. M., LUND, F. E. & SANZ, I. 2018. Distinct Effector B Cells Induced by Unregulated Toll-like Receptor 7 Contribute to Pathogenic Responses in Systemic Lupus Erythematosus. *Immunity,* 49**,** 725-739 e6.

LAU, D., LAN, L. Y., ANDREWS, S. F., HENRY, C., ROJAS, K. T., NEU, K. E., HUANG, M., HUANG, Y., DEKOSKY, B., PALM, A. E., IPPOLITO, G. C., GEORGIOU, G. & WILSON, P. C. 2017. Low CD21 expression defines a population of recent germinal center graduates primed for plasma cell differentiation. *Sci Immunol,* 2.

LI, S., MIAO, T., SEBASTIAN, M., BHULLAR, P., GHAFFARI, E., LIU, M., SYMONDS, A. L. & WANG, P. 2012. The transcription factors Egr2 and Egr3 are essential for the control of inflammation and antigen-induced proliferation of B and T cells. *Immunity,* 37**,** 685-96.

LIU, D., XU, H., SHIH, C., WAN, Z., MA, X., MA, W., LUO, D. & QI, H. 2015. T-B-cell entanglement and ICOSL-driven feed-forward regulation of germinal centre reaction. *Nature,* 517**,** 214-8.

LUN, A. T. L., RIESENFELD, S., ANDREWS, T., DAO, T. P., GOMES, T., PARTICIPANTS IN THE 1ST HUMAN CELL ATLAS, J. & MARIONI, J. C. 2019. EmptyDrops: distinguishing cells from empty droplets in droplet-based single-cell RNA sequencing data. *Genome Biol,* 20**,** 63.

MARKLIN, M., HEITMANN, J. S., FUCHS, A. R., TRUCKENMULLER, F. M., GUTKNECHT, M., BUGL, S., SAUR, S. J., LAZARUS, J., KOHLHOFER, U., QUINTANILLA-MARTINEZ, L., RAMMENSEE, H. G., SALIH, H. R., KOPP, H. G., HAAP, M., KIRSCHNIAK, A., KANZ, L., RAO,

A., WIRTHS, S. & MULLER, M. R. 2017. NFAT2 is a critical regulator of the anergic phenotype in chronic lymphocytic leukaemia. *Nat Commun,* 8**,** 755.

MERRELL, K. T., BENSCHOP, R. J., GAULD, S. B., AVISZUS, K., DECOTE-RICARDO, D., WYSOCKI, L. J. & CAMBIER, J. C. 2006. Identification of anergic B cells within a wild-type repertoire. *Immunity,* 25**,** 953-62.

MIOSGE, L. A., BLASIOLI, J., BLERY, M. & GOODNOW, C. C. 2002. Analysis of an ethylnitrosourea-generated mouse mutation defines a cell intrinsic role of nuclear factor kappaB2 in regulating circulating B cell numbers. *J Exp Med,* 196**,** 1113-9.

MOIR, S., HO, J., MALASPINA, A., WANG, W., DIPOTO, A. C., O'SHEA, M. A., ROBY, G., KOTTILIL, S., ARTHOS, J., PROSCHAN, M. A., CHUN, T. W. & FAUCI, A. S. 2008. Evidence for HIV-associated B cell exhaustion in a dysfunctional memory B cell compartment in HIV-infected viremic individuals. *J Exp Med,* 205**,** 1797-805.

MOIR, S., MALASPINA, A., OGWARO, K. M., DONOGHUE, E. T., HALLAHAN, C. W., EHLER, L. A., LIU, S., ADELSBERGER, J., LAPOINTE, R., HWU, P., BASELER, M., ORENSTEIN, J. M., CHUN, T. W., MICAN, J. A. & FAUCI, A. S. 2001. HIV-1 induces phenotypic and functional perturbations of B cells in chronically infected individuals. *Proc Natl Acad Sci U S A,* 98**,** 10362-7.

MORATTO, D., GULINO, A. V., FONTANA, S., MORI, L., PIROVANO, S., SORESINA, A., MEINI, A., IMBERTI, L., NOTARANGELO, L. D., PLEBANI, A. & BADOLATO, R. 2006. Combined decrease of defined B and T cell subsets in a group of common variable immunodeficiency patients. *Clin Immunol,* 121**,** 203-14.

NEWTON, J. S., LI, J., NING, Z. Q., SCHOENDORF, D. E., NORTON, J. D. & MURPHY, J. J. 1996. B cell early response gene expression coupled to B cell receptor, CD40 and interleukin-4 receptor co-stimulation: evidence for a role of the egr-2/krox 20 transcription factor in B cell proliferation. *Eur J Immunol,* 26**,** 811-6.

NICHOLS, E. M., JONES, R., WATSON, R., PEPPER, C. J., FEGAN, C. & MARCHBANK, K. J. 2015. A CD21 low phenotype, with no evidence of autoantibodies to complement proteins, is consistent with a poor prognosis in CLL. *Oncotarget,* 6**,** 32669-80.

OKAMOTO, M., MURAKAMI, M., SHIMIZU, A., OZAKI, S., TSUBATA, T., KUMAGAI, S. & HONJO, T. 1992. A transgenic model of autoimmune hemolytic anemia. *J Exp Med,* 175**,** 71-9.

QUACH, T. D., MANJARREZ-ORDUNO, N., ADLOWITZ, D. G., SILVER, L., YANG, H., WEI, C., MILNER, E. C. & SANZ, I. 2011. Anergic responses characterize a large fraction of human autoreactive naive B cells expressing low levels of surface IgM. *J Immunol,* 186**,** 4640-8.

RAKHMANOV, M., KELLER, B., GUTENBERGER, S., FOERSTER, C., HOENIG, M., DRIESSEN, G., VAN DER BURG, M., VAN DONGEN, J. J., WIECH, E., VISENTINI, M., QUINTI, I., PRASSE, A., VOELXEN, N., SALZER, U., GOLDACKER, S., FISCH, P., EIBEL, H., SCHWARZ, K., PETER, H. H. & WARNATZ, K. 2009. Circulating CD21low B cells in common variable immunodeficiency resemble tissue homing, innate-like B cells. *Proc Natl Acad Sci U S A,* 106**,** 13451-6.

RICKERT, R. C., ROES, J. & RAJEWSKY, K. 1997. B lymphocyte-specific, Cre-mediated mutagenesis in mice. *Nucleic Acids Res,* 25**,** 1317-8.

RITCHIE, M. E., PHIPSON, B., WU, D., HU, Y., LAW, C. W., SHI, W. & SMYTH, G. K. 2015. limma powers differential expression analyses for RNA-sequencing and microarray studies. *Nucleic Acids Res,* 43**,** e47.

RUBTSOV, A. V., RUBTSOVA, K., FISCHER, A., MEEHAN, R. T., GILLIS, J. Z., KAPPLER, J. W. & MARRACK, P. 2011. Toll-like receptor 7 (TLR7)-driven accumulation of a novel CD11c(+) B-cell population is important for the development of autoimmunity. *Blood,* 118**,** 1305-15.

RUBTSOVA, K., RUBTSOV, A. V., CANCRO, M. P. & MARRACK, P. 2015. Age-Associated B Cells: A T-bet-Dependent Effector with Roles in Protective and Pathogenic Immunity. *J Immunol,* 195**,** 1933-7.

RUSSELL KNODE, L. M., NARADIKIAN, M. S., MYLES, A., SCHOLZ, J. L., HAO, Y., LIU, D., FORD, M. L., TOBIAS, J. W., CANCRO, M. P. & GEARHART, P. J. 2017. Age-Associated B Cells Express a Diverse Repertoire of VH and Vkappa Genes with Somatic Hypermutation. *J Immunol,* 198**,** 1921-1927.

SABOURI, Z., PEROTTI, S., SPIERINGS, E., HUMBURG, P., YABAS, M., BERGMANN, H., HORIKAWA, K., ROOTS, C., LAMBE, S., YOUNG, C., ANDREWS, T. D., FIELD, M., ENDERS, A., REED, J. H. & GOODNOW, C. C. 2016. IgD attenuates the IgM-induced anergy response in transitional and mature B cells. *Nat Commun,* 7**,** 13381.

SCHARER, C. D., BLALOCK, E. L., MI, T., BARWICK, B. G., JENKS, S. A., DEGUCHI, T., CASHMAN, K. S., NEARY, B. E., PATTERSON, D. G., HICKS, S. L., KHOSROSHAHI, A., EUN-HYUNG LEE, F., WEI, C., SANZ, I. & BOSS, J. M. 2019. Epigenetic programming underpins B cell dysfunction in human SLE. *Nat Immunol,* 20**,** 1071-1082.

SCHUH, K., AVOTS, A., TONY, H. P., SERFLING, E. & KNEITZ, C. 1996. Nuclear NF-ATp is a hallmark of unstimulated B cells from B-CLL patients. *Leuk Lymphoma,* 23**,** 583-92.

SCHWERD, T., TWIGG, S. R. F., ASCHENBRENNER, D., MANRIQUE, S., MILLER, K. A., TAYLOR, I. B., CAPITANI, M., MCGOWAN, S. J., SWEENEY, E., WEBER, A., CHEN, L., BOWNESS, P., RIORDAN, A., CANT, A., FREEMAN, A. F., MILNER, J. D., HOLLAND, S. M., FREDE, N., MULLER, M., SCHMIDT-ARRAS, D., GRIMBACHER, B., WALL, S. A., JONES, E. Y., WILKIE, A. O. M. & UHLIG, H. H. 2017. A biallelic mutation in IL6ST encoding the GP130 co-receptor causes immunodeficiency and craniosynostosis. *J Exp Med,* 214**,** 2547-2562.

SHIROGANE, T., FUKADA, T., MULLER, J. M., SHIMA, D. T., HIBI, M. & HIRANO, T. 1999. Synergistic roles for Pim-1 and c-Myc in STAT3-mediated cell cycle progression and antiapoptosis. *Immunity,* 11**,** 709-19.

TAILLEBOURG, E., BUART, S. & CHARNAY, P. 2002. Conditional, floxed allele of the Krox20 gene. *Genesis,* 32**,** 112-3.

TANGYE, S. G. & MA, C. S. 2020. Regulation of the germinal center and humoral immunity by interleukin-21. *J Exp Med,* 217.

TERRIER, B., JOLY, F., VAZQUEZ, T., BENECH, P., ROSENZWAJG, M., CARPENTIER, W., GARRIDO, M., GHILLANI-DALBIN, P., KLATZMANN, D., CACOUB, P. & SAADOUN, D. 2011. Expansion of functionally anergic CD21-/low marginal zone-like B cell clones in hepatitis C virus infection-related autoimmunity. *J Immunol,* 187**,** 6550-63.

TOURTELLOTTE, W. G. & MILBRANDT, J. 1998. Sensory ataxia and muscle spindle agenesis in mice lacking the transcription factor Egr3. *Nat Genet,* 20**,** 87-91.

TSAI, C. M., CHIU, Y. K., HSU, T. L., LIN, I. Y., HSIEH, S. L. & LIN, K. I. 2008. Galectin-1 promotes immunoglobulin production during plasma cell differentiation. *J Immunol,* 181**,** 4570-9.

WARNATZ, K., WEHR, C., DRAGER, R., SCHMIDT, S., EIBEL, H., SCHLESIER, M. & PETER, H. H. 2002. Expansion of CD19(hi)CD21(lo/neg) B cells in common variable immunodeficiency (CVID) patients with autoimmune cytopenia. *Immunobiology,* 206**,** 502-13.

WEI, C., ANOLIK, J., CAPPIONE, A., ZHENG, B., PUGH-BERNARD, A., BROOKS, J., LEE, E. H., MILNER, E. C. & SANZ, I. 2007. A new population of cells lacking expression of CD27 represents a notable component of the B cell memory compartment in systemic lupus erythematosus. *J Immunol,* 178**,** 6624-33.

WILLIAMS, J. B., HORTON, B. L., ZHENG, Y., DUAN, Y., POWELL, J. D. & GAJEWSKI, T. F. 2017. The EGR2 targets LAG-3 and 4-1BB describe and regulate dysfunctional antigen-specific CD8+ T cells in the tumor microenvironment. *J Exp Med,* 214**,** 381-400.

947 WONG, S. C., CHEW, W. K., TAN, J. E., MELENDEZ, A. J., FRANCIS, F. & LAM, K. P. 2002.
948 Peritoneal CD5+ B-1 cells have signaling properties similar to tolerant B cells. *J Biol*
949 *Chem,* 277**,** 30707-15.
950 YOON, H. S., SCHARER, C. D., MAJUMDER, P., DAVIS, C. W., BUTLER, R., ZINZOW-KRAMER, W.,
951 SKOUNTZOU, I., KOUTSONANOS, D. G., AHMED, R. & BOSS, J. M. 2012. ZBTB32 is an
952 early repressor of the CIITA and MHC class II gene expression during B cell
953 differentiation to plasma cells. *J Immunol,* 189**,** 2393-403.
954 YOUNG, E., NOERENBERG, D., MANSOURI, L., LJUNGSTROM, V., FRICK, M., SUTTON, L. A.,
955 BLAKEMORE, S. J., GALAN-SOUSA, J., PLEVOVA, K., BALIAKAS, P., ROSSI, D., CLIFFORD,
956 R., ROOS-WEIL, D., NAVRKALOVA, V., DORKEN, B., SCHMITT, C. A., SMEDBY, K. E.,
957 JULIUSSON, G., GIACOPELLI, B., BLACHLY, J. S., BELESSI, C., PANAGIOTIDIS, P.,
958 CHIORAZZI, N., DAVI, F., LANGERAK, A. W., OSCIER, D., SCHUH, A., GAIDANO, G., GHIA,
959 P., XU, W., FAN, L., BERNARD, O. A., NGUYEN-KHAC, F., RASSENTI, L., LI, J., KIPPS, T. J.,
960 STAMATOPOULOS, K., POSPISILOVA, S., ZENZ, T., OAKES, C. C., STREFFORD, J. C.,
961 ROSENQUIST, R. & DAMM, F. 2017. EGR2 mutations define a new clinically aggressive
962 subgroup of chronic lymphocytic leukemia. *Leukemia,* 31**,** 1547-1554.
963 ZHANG, Y., LIU, T., MEYER, C. A., EECKHOUTE, J., JOHNSON, D. S., BERNSTEIN, B. E., NUSBAUM,
964 C., MYERS, R. M., BROWN, M., LI, W. & LIU, X. S. 2008. Model-based analysis of ChIP-Seq
965 (MACS). *Genome Biol,* 9**,** R137.
966 ZIKHERMAN, J., PARAMESWARAN, R. & WEISS, A. 2012. Endogenous antigen tunes the
967 responsiveness of naive B cells but not T cells. *Nature,* 489**,** 160-4.
968

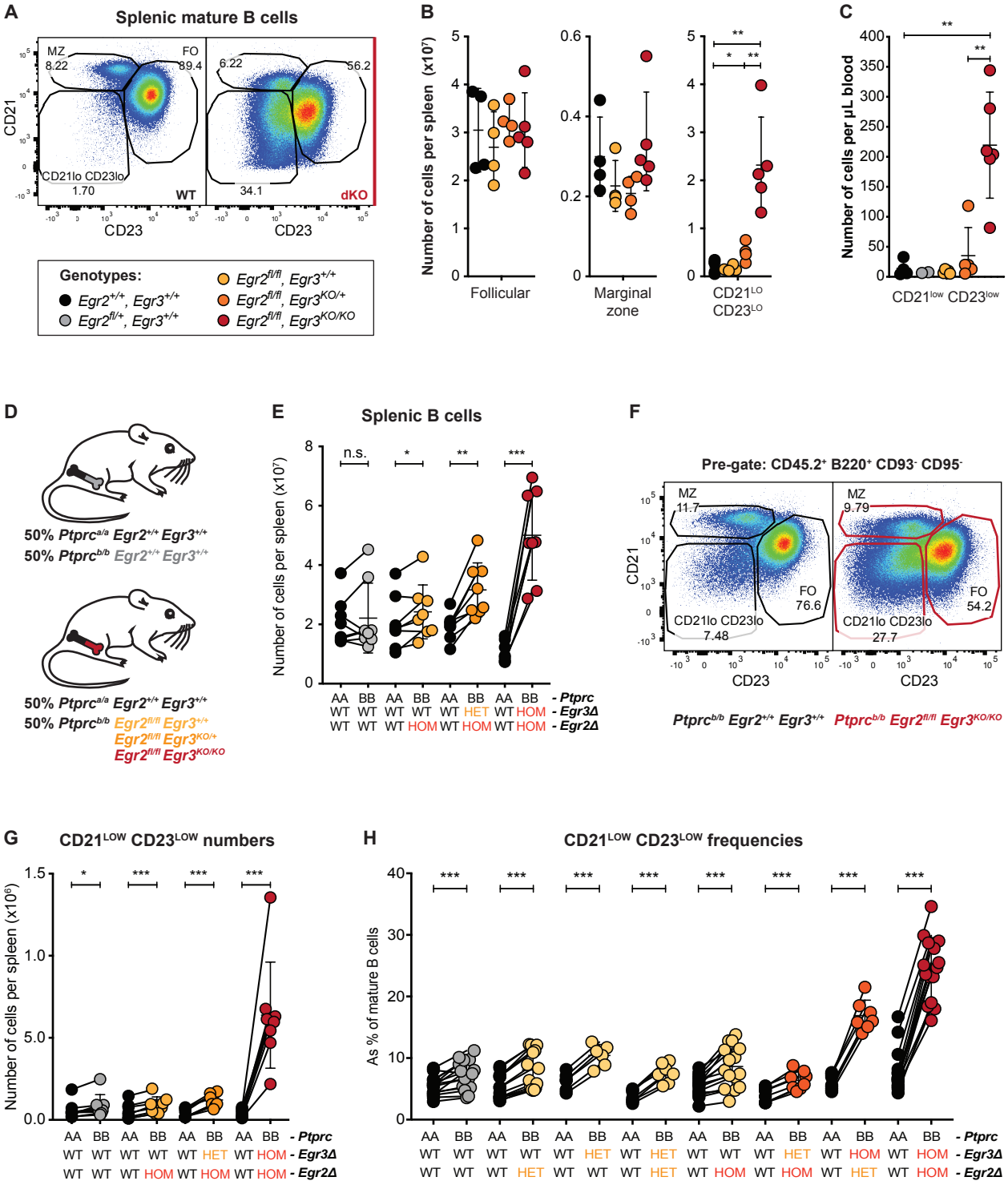
A
Splenic mature B cells
MZ
8.22
FO
89.4
CD21lo CD23lo
1.70
WT
6.22
56.2
34.1
dKO
CD21
CD23
CD23
Genotypes:
Egr2+/+, Egr3+/+
Egr2fl/+, Egr3+/+
Egr2fl/fl, Egr3+/+
Egr2fl/fl, Egr3KO/+
Egr2fl/fl, Egr3KO/KO
B
Number of cells per spleen (x10⁷)
Follicular
Marginal zone
CD21LO CD23LO
C
Number of cells per µL blood
CD21low CD23low
D
50% Ptprca/a Egr2+/+ Egr3+/+
50% Ptprcb/b Egr2+/+ Egr3+/+
50% Ptprca/a Egr2+/+ Egr3+/+
50% Ptprcb/b Egr2fl/fl Egr3+/+
Egr2fl/fl Egr3KO/+
Egr2fl/fl Egr3KO/KO
E
Splenic B cells
n.s.
Number of cells per spleen (x10⁷)
AA BB AA BB AA BB AA BB - Ptprc
WT WT WT WT WT HET WT HOM - Egr3Δ
WT WT WT HOM WT HOM WT HOM - Egr2Δ
F
Pre-gate: CD45.2+ B220+ CD93- CD95-
MZ
11.7
FO
76.6
CD21lo CD23lo
7.48
MZ
9.79
FO
54.2
CD21lo CD23lo
27.7
CD21
CD23
CD23
Ptprcb/b Egr2+/+ Egr3+/+
Ptprcb/b Egr2fl/fl Egr3KO/KO
G
CD21LOW CD23LOW numbers
Number of cells per spleen (x10⁶)
AA BB AA BB AA BB AA BB - Ptprc
WT WT WT WT WT HET WT HOM - Egr3Δ
WT WT WT HOM WT HOM WT HOM - Egr2Δ
H
CD21LOW CD23LOW frequencies
As % of mature B cells
AA BB AA BB AA BB AA BB AA BB AA BB AA BB AA BB - Ptprc
WT WT WT WT WT HET WT HET WT WT WT HET WT HOM WT HOM - Egr3Δ
WT WT WT HET WT WT WT HET WT HOM WT HOM WT HET WT HOM - Egr2Δ

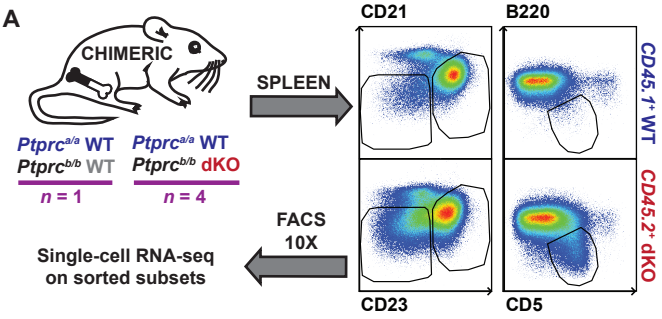
A
CHIMERIC
Ptprc a/a WT
Ptprc b/b WT
n = 1
Ptprc a/a WT
Ptprc b/b dKO
n = 4
SPLEEN
FACS
10X
Single-cell RNA-seq
on sorted subsets
CD21
B220
CD23
CD5
CD45.1+ WT
CD45.2+ dKO

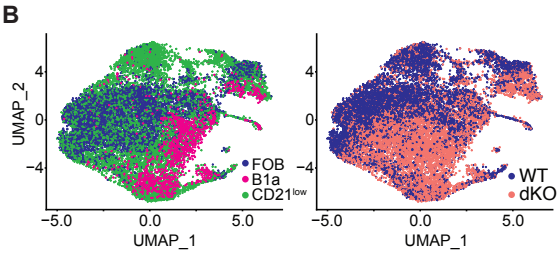
B
UMAP_2
UMAP_1
FOB
B1a
CD21low
WT
dKO

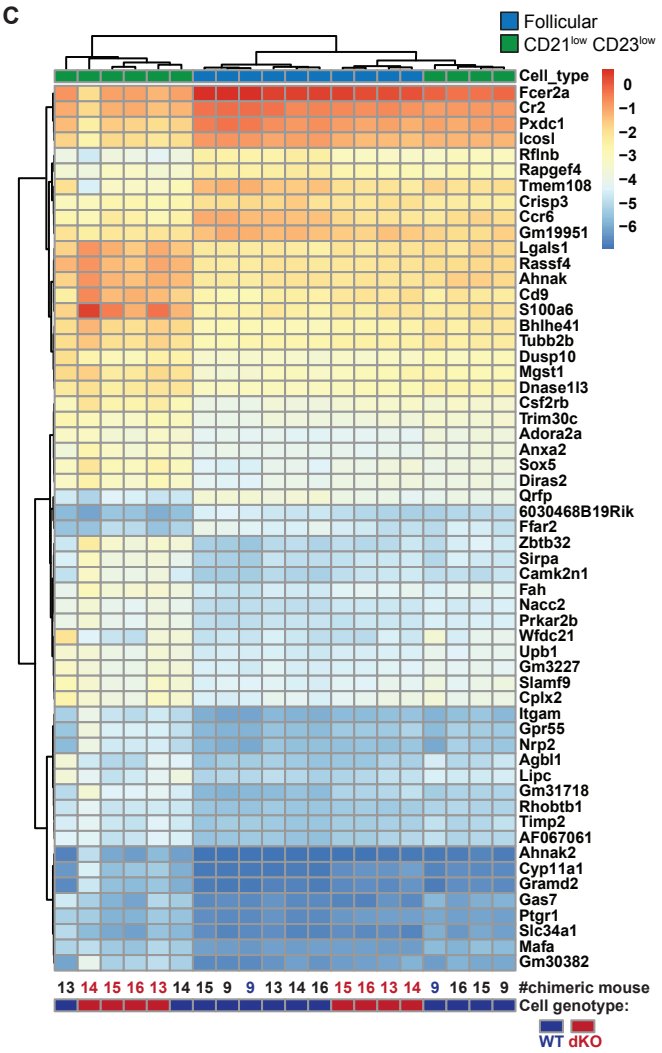
C
Follicular
CD21low CD23low
Cell_type
Fcer2a
Cr2
Pxdc1
Icosl
Rflnb
Rapgef4
Tmem108
Crisp3
Ccr6
Gm19951
Lgals1
Rassf4
Ahnak
Cd9
S100a6
Bhlhe41
Tubb2b
Dusp10
Mgst1
Dnase1l3
Csf2rb
Trim30c
Adora2a
Anxa2
Sox5
Diras2
Qrfp
6030468B19Rik
Ffar2
Zbtb32
Sirpa
Camk2n1
Fah
Nacc2
Prkar2b
Wfdc21
Upb1
Gm3227
Slamf9
Cplx2
Itgam
Gpr55
Nrp2
Agbl1
Lipc
Gm31718
Rhobtb1
Timp2
AF067061
Ahnak2
Cyp11a1
Gramd2
Gas7
Ptgr1
Slc34a1
Mafa
Gm30382
13 14 15 16 13 14 15 9 9 13 14 16 15 16 13 14 9 16 15 9
#chimeric mouse
Cell genotype:
WT dKO

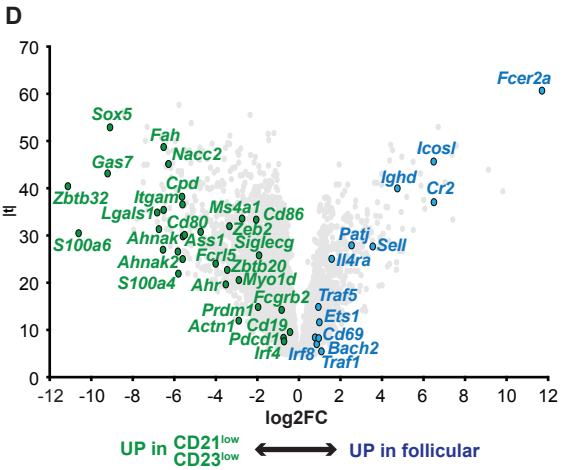
D
|t|
log2FC
Fcer2a
Sox5
Fah
Nacc2
Gas7
Cpd
Zbtb32
Itgam
Lgals1
Ms4a1
Cd86
Cd80
Zeb2
S100a6
Ahnak
Ass1
Siglecg
Fcrl5
Ahnak2
Zbtb20
S100a4
Myo1d
Ahr
Fcgrb2
Traf5
Prdm1
Ets1
Actn1
Cd19
Cd69
Pdcd1
Bach2
Irf4
Irf8
Traf1
Icosl
Ighd
Cr2
Patj
Sell
Il4ra
UP in CD21low CD23low
UP in follicular

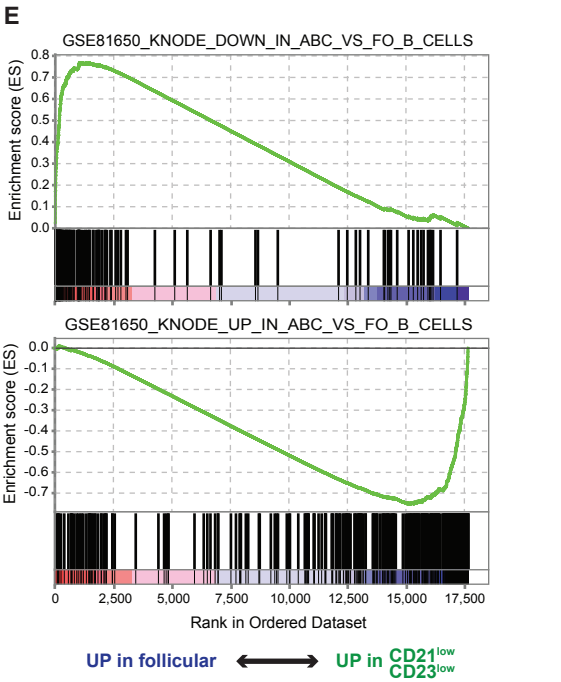
E
GSE81650_KNODE_DOWN_IN_ABC_VS_FO_B_CELLS
Enrichment score (ES)
GSE81650_KNODE_UP_IN_ABC_VS_FO_B_CELLS
Enrichment score (ES)
Rank in Ordered Dataset
UP in follicular
UP in CD21low CD23low

A

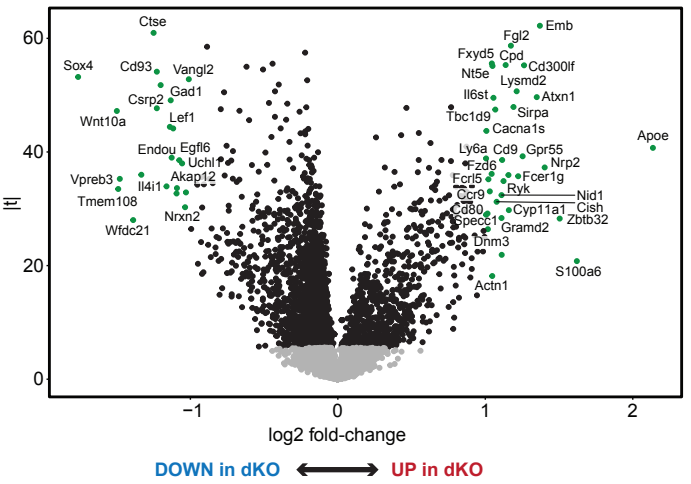

B

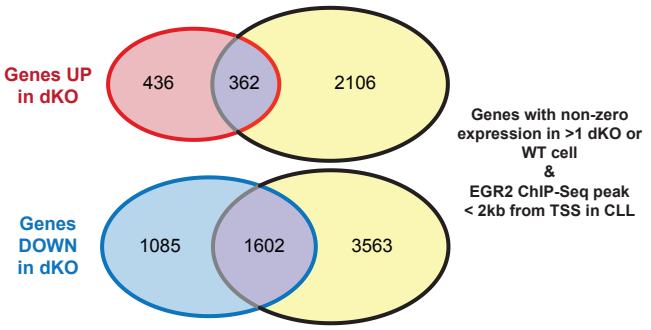

C

DOWN in dKO

Gene	Log2FC
Wnt10a	-1.50
Vpreb3	-1.48
Il4i1	-1.16
Lef1	-1.14
Nrxn2	-1.09
Map2	-0.93
Nrgn	-0.92
Gm16867	-0.89
Tsc22d1	-0.81
Fcer2a	-0.78
Id3	-0.74
Gfod1	-0.74
Il12a	-0.74
Rapgefl1	-0.73
Hes1	-0.72
Itgb3	-0.71
Il21r	-0.71
Frat2	-0.69
Bmf	-0.67
Dusp2	-0.63
Plk2	-0.63
Blvrb	-0.62
Pdzd2	-0.61
Gm37306	-0.59
Cnn3	-0.58
Icosl	-0.58
Stmn1	-0.58
Tnfrsf13c	-0.57
Zfp318	-0.57
Brwd1	-0.55
Them6	-0.54
Nfkb2	-0.54
Egr3	-0.52
Zdhhc14	-0.51
Gpr146	-0.51
Fanca	-0.48
Spib	-0.47
Serinc5	-0.47
Otud1	-0.46
Scimp	-0.45

UP in dKO

Gene	Log2FC
Zbtb32	1.50
Emb	1.37
Atxn1	1.35
Lysmd2	1.21
Cpd	1.14
Cish	1.08
Tbc1d9	1.07
Il6st	1.06
Specc1	1.01
Zbtb20	0.88
Rcn3	0.86
5033430I15Rik	0.83
S100a4	0.78
Pde8a	0.77
Gm10645	0.76
Sytl1	0.76
Tmem141	0.75
Fam46c	0.71
Epn2	0.70
Itgb1	0.70
Kcnn4	0.67
Myo1d	0.65
Dtx1	0.64
Slfn1	0.64
Tmem154	0.63
Lgals1	0.62
Lmo7	0.62
Prodh	0.62
Dok2	0.62
Ahnak	0.62
Atf3	0.61
Plekha8	0.60
Plcd3	0.59
Dkkl1	0.57
Il6ra	0.56
Rab20	0.56
Gm45669	0.55
Mzb1	0.55
Ptms	0.54
Rgmb	0.53

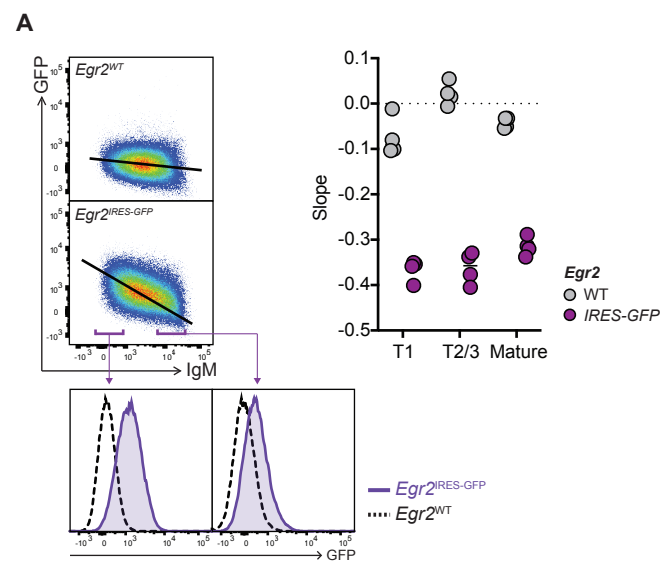

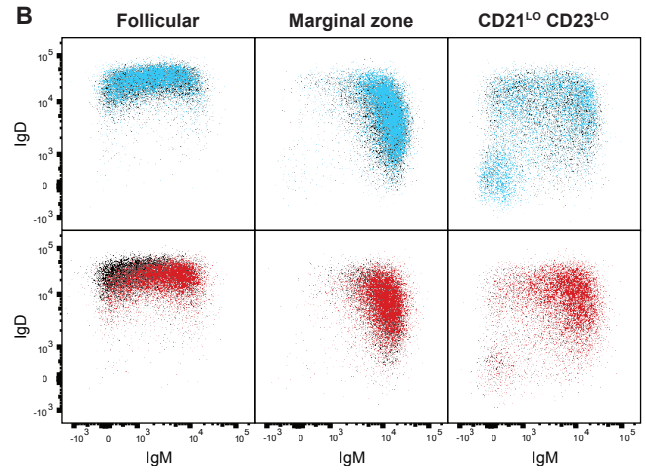

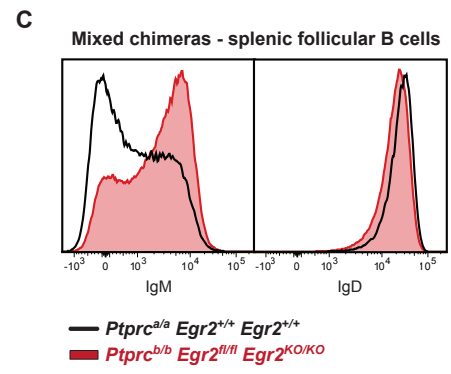

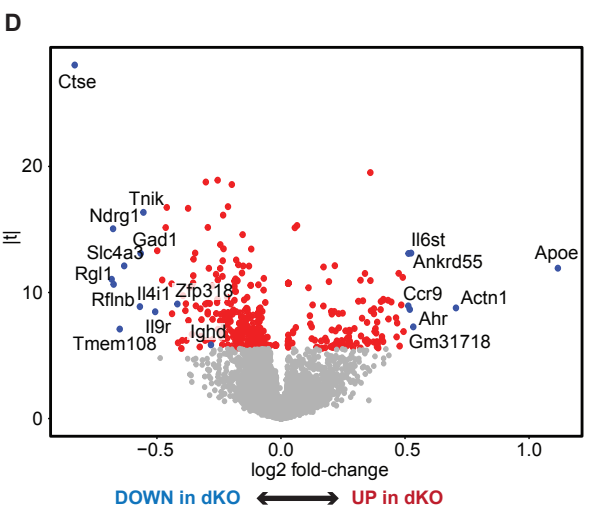

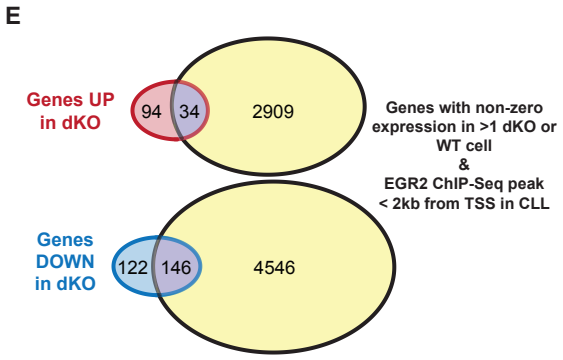

F

Down in dKO		Up in dKO	
Gene	log2FC	Gene	log2FC
Rgl1	-0.68	Actn1	0.71
Ndrg1	-0.68	Il6st	0.52
Il4i1	-0.57	Cpd	0.49
Tnik	-0.55	Nectin1	0.47
Crip3	-0.48	Emb	0.46
Zfp318	-0.46	Cyb5r2	0.44
Gm16867	-0.46	Lysmd2	0.41
Slc4a11	-0.44	Ctla4	0.39
Tsc22d1	-0.38	Mzb1	0.36
Xkrx	-0.36	5033430I15Rik	0.36
Il21r	-0.35	Myo1d	0.34
Scimp	-0.35	Smco4	0.34
Gsn	-0.35	Sbf2	0.33
Itgb3	-0.34	Dtx1	0.33
Icosl	-0.33	Stk3	0.31
Fchsd2	-0.32	Mcoln2	0.27
Nfkb2	-0.28	Prodh	0.27
Frat2	-0.27	Pde8a	0.25
Fam212a	-0.26	Arhgap24	0.24
Map7	-0.26	Pde4a	0.24
Dexi	-0.25	Rasal1	0.22
Kctd12	-0.24	Gns	0.22
Rara	-0.24	Rab37	0.21
Psd	-0.24	Lgmn	0.20

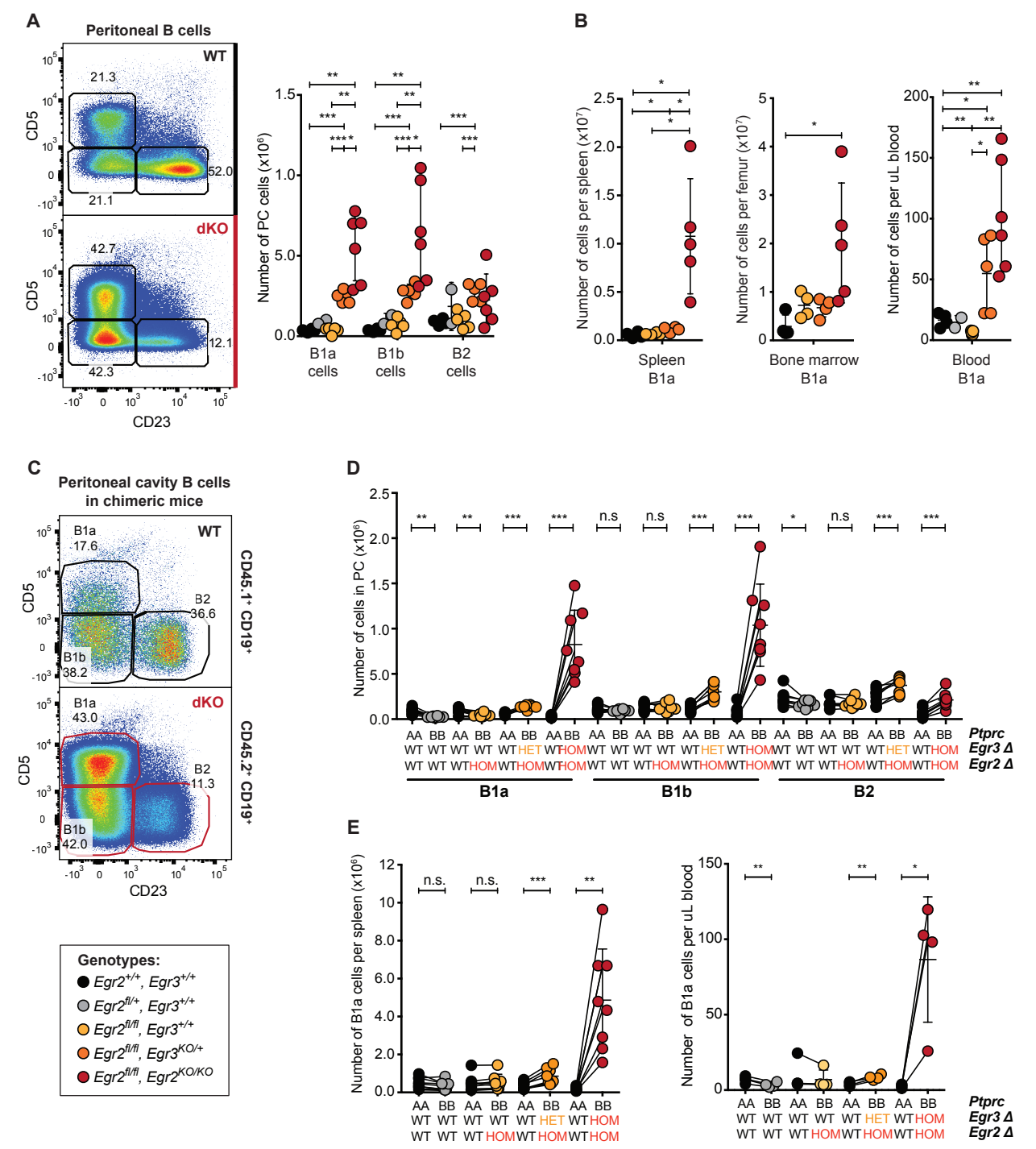
A
Peritoneal B cells
WT
dKO
CD5
CD23
21.3
52.0
21.1
42.7
12.1
42.3
Number of PC cells (x10⁶)
B1a cells
B1b cells
B2 cells
B
Number of cells per spleen (x10⁷)
Spleen B1a
Number of cells per femur (x10⁷)
Bone marrow B1a
Number of cells per uL blood
Blood B1a
C
Peritoneal cavity B cells in chimeric mice
B1a 17.6
B2 36.6
B1b 38.2
B1a 43.0
B2 11.3
B1b 42.0
CD45.1⁺ CD19⁺
CD45.2⁺ CD19⁺
Genotypes:
Egr2+/+, Egr3+/+
Egr2fl/+, Egr3+/+
Egr2fl/fl, Egr3+/+
Egr2fl/fl, Egr3KO/+
Egr2fl/fl, Egr2KO/KO
D
Number of cells in PC (x10⁶)
B1a
B1b
B2
Ptprc
Egr3 Δ
Egr2 Δ
E
Number of B1a cells per spleen (x10⁶)
Number of B1a cells per uL blood

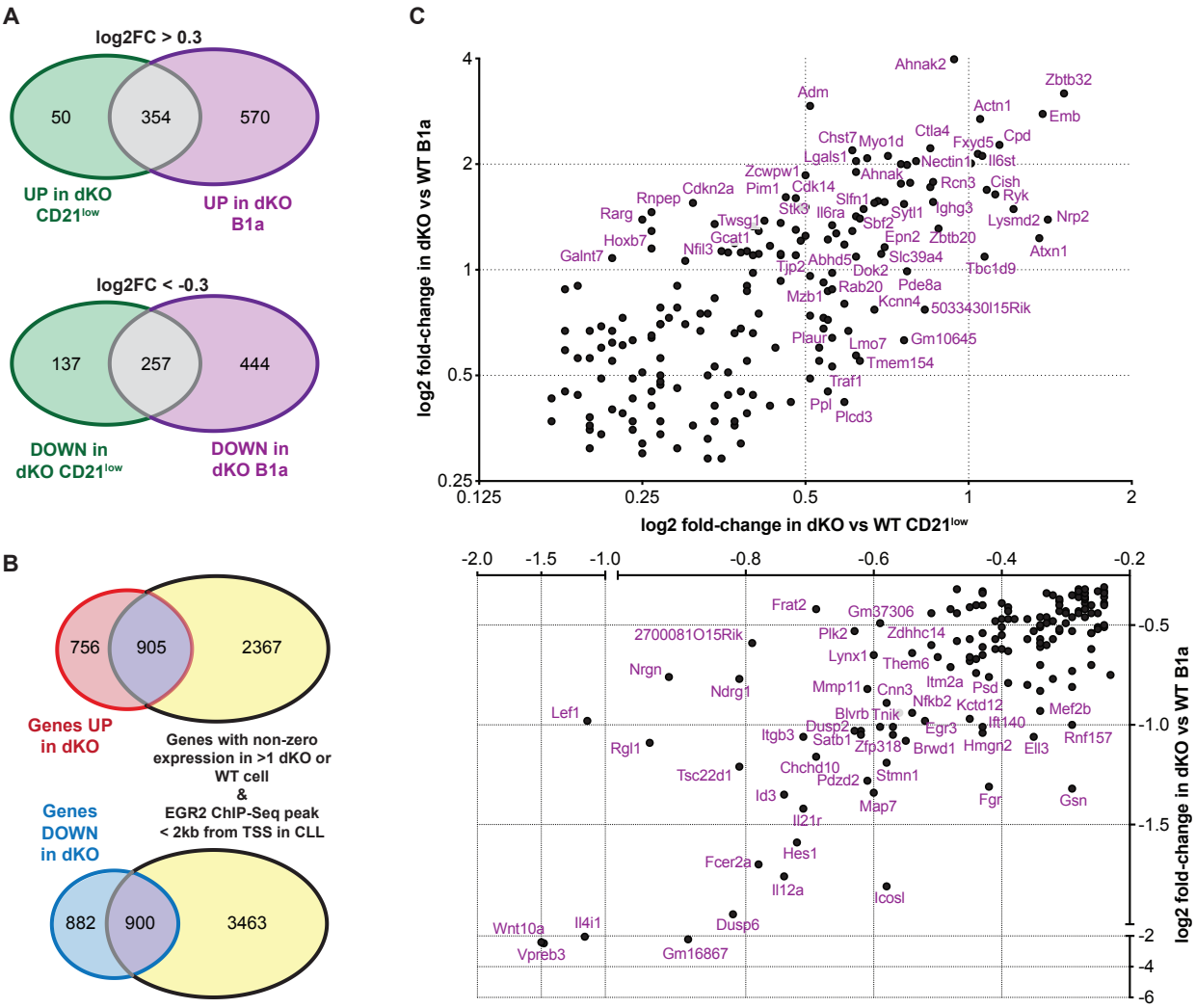
A
log2FC > 0.3
50
354
570
UP in dKO CD21low
UP in dKO B1a
log2FC < -0.3
137
257
444
DOWN in dKO CD21low
DOWN in dKO B1a
B
756
905
2367
Genes UP in dKO
Genes with non-zero expression in >1 dKO or WT cell
&
EGR2 ChIP-Seq peak < 2kb from TSS in CLL
Genes DOWN in dKO
882
900
3463
C
log2 fold-change in dKO vs WT B1a
log2 fold-change in dKO vs WT CD21low
Ahnak2
Zbtb32
Adm
Actn1
Emb
Chst7
Myo1d
Ctla4
Fxyd5
Cpd
Lgals1
Nectin1
Il6st
Zcwpw1
Ahnak
Rcn3
Cish
Pim1
Cdk14
Ryk
Rnpep
Cdkn2a
Slfn1
Rarg
Stk3
Il6ra
Sytl1
Ighg3
Lysmd2
Nrp2
Twsg1
Sbf2
Hoxb7
Gcat1
Epn2
Zbtb20
Atxn1
Galnt7
Nfil3
Abhd5
Slc39a4
Tjp2
Dok2
Tbc1d9
Rab20
Pde8a
Mzb1
Kcnn4
5033430I15Rik
Plaur
Lmo7
Gm10645
Tmem154
Traf1
Ppl
Plcd3
Frat2
Gm37306
2700081O15Rik
Plk2
Zdhhc14
Lynx1
Them6
Nrgn
Ndrg1
Mmp11
Cnn3
Itm2a
Psd
Nfkb2
Kctd12
Lef1
Blvrb
Tnik
Mef2b
Dusp2
Egr3
Ift140
Itgb3
Satb1
Zfp318
Brwd1
Hmgn2
Ell3
Rnf157
Rgl1
Chchd10
Tsc22d1
Pdzd2
Stmn1
Id3
Map7
Fgr
Gsn
Il21r
Hes1
Fcer2a
Il12a
Icosl
Wnt10a
Il4i1
Dusp6
Vpreb3
Gm16867